AD-A054 857   DAYTON UNIV OHIO RESEARCH INST   F/G 7/2
FEASIBILITY STUDY OF INORGANIC OXIDES FOR THERMAL ENERGY STORAG--ETC(U)
NOV 77 J E DAVISON   F33615-76-C-2096
UNCLASSIFIED   UDRI-TR-77-53   AFAPL-TR-77-70   NL

| OF
AD
A054857

END
DATE
FILMED
7-78
DDC

FOR FURTHER TRAN~~...~~

AFAPL-TR-77-70

AD A054857

FEASIBILITY STUDY OF INORGANIC OXIDES FOR THERMAL ENERGY STORAGE APPLICATIONS.

UNIVERSITY OF DAYTON RESEARCH INSTITUTE
DAYTON, OHIO

Joseph E. / Davison

NOV 77

UDRI-TR-77-53

D D C

RECEIVED
JUN 8 1978
E

87 p.

TECHNICAL REPORT AFAPL-TR-77-70
Final Report. 15 Mar 1976 – 30 Sep 77

F33615-76-C-2096

3145

19

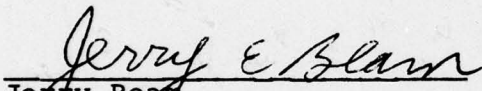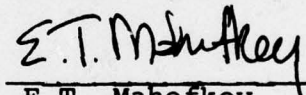Approved for public release; distribution unlimited.

105400

NOTICE

When Government drawings, specifications, or other data are used for any purpose other than in connection with a definitely related Government procurement operation, the United States Government thereby incurs no responsibility nor any obligation whatsoever; and the fact that the government may have formulated, furnished, or in any way supplied the said drawings, specifications, or other data, is not to be regarded by implication or otherwise as in any manner licensing the holder or any other person or corporation, or conveying any rights or permission to manufacture, use, or sell any patented invention that may in any way be related thereto.
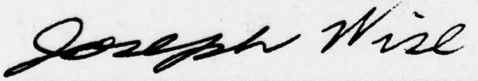
This report has been reviewed by the Information Office (OI) and is releasable to the National Technical Information Service (NTIS). At NTIS, it will be available to the general public, including foreign nations.

This technical report has been reviewed and is approved for publication.

Jerry Beam
Project Engineer

E.T. Mahefkey
Project Engineer

FOR THE COMMANDER

Joseph F. Wise
Technical Area Manager
Energy Conversion Branch

REPORT DOCUMENTATION PAGE		READ INSTRUCTIONS BEFORE COMPLETING FORM
1. REPORT NUMBER AFAPL-TR-77-70	2. GOVT ACCESSION NO.	3. RECIPIENT'S CATALOG NUMBER
4. TITLE *(and Subtitle)* "FEASIBILITY STUDY OF INORGANIC OXIDES FOR THERMAL ENERGY STORAGE APPLICATIONS"		5. TYPE OF REPORT & PERIOD COVERED Final Report Mar 1976 to Sept 1977
		6. PERFORMING ORG. REPORT NUMBER UDR-TR-77-53
7. AUTHOR(s) Dr. Joseph E. Davison		8. CONTRACT OR GRANT NUMBER(s) F33615-76-C-2096 New
9. PERFORMING ORGANIZATION NAME AND ADDRESS University of Dayton univ., Ohio. Research Inst. 300 College Park, Dayton, Ohio 45469		10. PROGRAM ELEMENT, PROJECT, TASK AREA & WORK UNIT NUMBERS P.E. 62203F, Proj. 3145, Task 314519, W.U.31451960
11. CONTROLLING OFFICE NAME AND ADDRESS Air Force Aero Propulsion Laboratory POE-2 Wright-Patterson AFB, Ohio 45433		12. REPORT DATE November 1977
		13. NUMBER OF PAGES 77
14. MONITORING AGENCY NAME & ADDRESS(*if different from Controlling Office*)		15. SECURITY CLASS. *(of this report)* Unclassified
		15a. DECLASSIFICATION/DOWNGRADING SCHEDULE

16. DISTRIBUTION STATEMENT *(of this Report)*

Approved for public release; distribution unlimited.

17. DISTRIBUTION STATEMENT *(of the abstract entered in Block 20, if different from Report)*

18. SUPPLEMENTARY NOTES

19. KEY WORDS *(Continue on reverse side if necessary and identify by block number)*

thermal energy storage, space power, thermal diffusivity, liquid density, heat of transformation

20. ABSTRACT *(Continue on reverse side if necessary and identify by block number)*

The University of Dayton conducted a feasibility study of the application of inorganic oxides as the best energy storage media for thermal energy storage devices. The thermophysical properties of the heat of fusion and the melting temperatures of the pure inorganic oxides were reviewed and evaluated. A total of nine inorganic oxides were identified which have a value for the heat of fusion greater than 793.7 Joules per gram (100 watt-hours per pound). However, all of the melting points of these

over

DD FORM 1473 1 JAN 73 EDITION OF 1 NOV 65 IS OBSOLETE

20. Abstract (cont'd)

nine oxides are greater than 1570°C. Since none of these pure materials had a melting point in the desired temperature interval of 538°C to 760°C (1000°F to 1400°F), the phase diagrams of binary inorganic oxides were reviewed. The study of binary inorganic oxide systems was limited to those systems which contain at least one of the nine pure oxides which have a liquid-solid transformation in the required temperature interval. The binary system comprised of dilithium oxide and diboron trioxide was assessed as having the highest potential. This assessment was based on the amount of dilithium oxide present in the eutectic composition. The value of the transformation temperature of the eutectic composition was verified by Differential Thermal Analysis as being 650°C. The value for the heat of the liquid-solid transformation was measured by the technique of Drop Calorimetry and found to be 414.1 joules per gram (52.18 watt-hours per pound). The value for the eutectic composition of the $LiF-MgF_2$ system was measured and found to be 530.3 joules per gram. The value of the ternary eutectic composition in the $LiF-MgF_2-KF$ was also measured and found to be 753.6 joules per gram (94.95 watt-hours per pound). Values for the density of the liquid phases were measured for the eutectic compositions in the systems of $Li_2O-B_2O_3$, $LiF-MgF_2$, LiF_3-MgF_2-KF, and $LiF-MgF_2-NaF$. The values which were found are:

$Li_2O-B_2O_3$	1.973 grams per cubic centimeter,
$LiF-MgF_2$	2.219 grams per cubic centimeter,
$LiF-MgF_2-KF$	2.182 grams per cubic centimeter,
$LiF-MgF_2-NaF$	2.215 grams per cubic centimeter.

The values for the thermal diffusivity were measured on these same systems in the solid phase as a function of temperature. The thermal diffusivity at 25°C of the eutectic fluorides were found to be:

$LiF-MgF_2-KF$	0.016 cm^2 per second,
$LiF-MgF_2-NaF$	0.013 cm^2 per second,
$Li_2O-B_2O_3$	0.0072 cm^2 per second,
$LiF-MgF_2$	0.013 cm^2 per second.

As a result of these studies, the eutectic fluoride compositions are considered to have a higher potential as the energy storage media than the eutectic oxides for the temperature interval of interest.

The chemical compatibility between inorganic oxides and container alloys was assessed by comparing the values of the Gibb's free energy for oxidation-reduction reactions. On this basis, stainless steel alloys and nickel-based superalloys which do not contain aluminum, magnesium, titanium, or silicon were judged to be satisfactory as containers of dilithium oxide and diboron trioxide eutectic compositions. Test specimens of the $Li_2O-B_2O_3$ eutectic composition were sealed in a nickel-based superalloy and are undergoing life testing to experimentally determine the chemical compatibility. The results of these experiments will be communicated in a separate report.

FOREWORD

This final report was submitted by the University of Dayton under Contract F33615-76-C-2096. The effort was sponsored by the Air Force Systems Command, Air Force Space and Missile Systems Division, El Segundo, California under Project Number 3145, Task 314519, Work Unit 31451960. The project engineers were Mr. Jerry Beam and Mr. E.T. Mahefkey of the Air Force Aero Propulsion Laboratory, Air Force Systems Command, Wright-Patterson Air Force Base, Ohio. The purpose of this project was to assess the feasibility of utilizing inorganic oxides for thermal energy storage applications for cryocoolers for space power systems. Joseph E. Davison of the University of Dayton was technically responsible for the work. The Air Force Materials Laboratory assisted in the welding of thermal energy storage units. The Dynatherm Corporation, Cockeysville, Maryland assisted in the filling and sealing of sodium heat pipe thermal energy storage reservoirs. The work covered the time period of March 1976 to September 1977.

iii

TABLE OF CONTENTS

LIST OF ILLUSTRATIONS

LIST OF TABLES

ix

SECTION I
INTRODUCTION AND SUMMARY

The University of Dayton has conducted a feasibility study
of the application of inorganic oxides as the best energy storage
media for thermal energy storage devices. The thermophysical pro-
perties of the heat of fusion and the melting temperatures of the
pure inorganic oxides were reviewed and evaluated. A total of
nine inorganic oxides were identified which have a value for the
heat of fusion greater than 100 watt-hours per pound (793.7 joules
per gram). However, all of the melting points of these nine
oxides are greater than 1570°C. Since none of these pure
materials had a melting point in the desired temperature interval
of 538°C to 760°C (1000°F to 1400°F), the phase diagrams of
binary inorganic oxides were reviewed. The study of binary in-
organic oxide systems was limited to those systems which contain
at least one of the nine pure oxides which have a liquid-solid
transformation in the required temperature interval. The binary
system comprised of dilithium oxide and diboron trioxide was
assessed as having the highest potential. This assessment was
based on the amount of dilithium oxide present in the eutectic
composition. The value of the transformation temperature of
the eutectic composition was verified by Differential Thermal
Analysis as being 650°C. The value for the heat of the liquid-
solid transformation was measured by the technique of Drop
Calorimetry and found to be 414.1 joules per gram. The value
of the eutectic composition in the $LiF-MgF_2$ was measured and
found to be 530.3 joules per gram. The value of the ternary
eutectic composition in the $LiF-MgF_2-KF$ was also measured and
found to be 753.6 joules per gram. Values for the density of
the liquid phases were measured for the eutectic compositions
in the systems of $Li_2O-B_2O_3$, $LiF-MgF_2$, $LiF-MgF_2-KF$, and $LiF-MgF_2-NaF$. The values which were found are:

$Li_2O-B_2O_3$	1.973 grams per cubic centimeter,
$LiF-MgF_2$	2.219 grams per cubic centimeter,

1

LiF-MgF$_2$-KF	2.182 grams per cubic centimeter,
LiF-MgF$_2$-NaF	2.215 grams per cubic centimeter.

The values for the thermal diffusivity were measured on these same systems in the solid phase as a function of temperature. The thermal diffusivity at 25°C of the eutectic fluorides were found to be:

LiF-MgF$_2$-KF	0.016 cm^2 per second,
LiF-MgF$_2$-NaF	0.013 cm^2 per second,
Li$_2$O-B$_2$O$_3$	0.0072 cm^2 per second,
LiF-MgF$_2$	0.013 cm^2 per second.

As a result of these studies, the eutectic fluoride compositions are considered to have a higher potential as the energy storage media than the eutectic oxides for the temperature interval of interest.

2

SECTION II
ANALYTICAL STUDIES

The purpose of this investigation was to experimentally demonstrate the feasibility of using the liquid-solid transformation of inorganic oxides to store heat energy for thermal energy storage (TES) units. The value for the heat of fusion was one of the properties used in selecting inorganic oxides. Oxides whose values are greater than 100 watt-hours per pound (793.7 joules per gram) are desired. The temperature range of immediate interest for the TES application was specified to be between 538 and 760°C. Thus, only liquid-solid transformations in that temperature interval are of interest. These two properties, the melting temperature and the heat of fusion, were specified to assure that the oxides would be candidate materials for the TES units to supply the thermal power for Vuilleumier cryocooler space vehicle applications. Our previous investigation had evaluated inorganic fluoride compositions which have potential for this application.* Finally, the compatibility of these oxides with suitable container materials was to be assessed.

2.1   TECHNICAL APPROACH

The approach which we used in selecting the inorganic oxides was to compare the values for the heat of fusion of these oxides. Those oxides which had values greater than 100 watt-hours per pound (793.7 joules per gram) were identified. The melting temperatures of the pure oxides were reviewed to determine which oxides melt in the desired interval (538-760°C). Next, the liquid-solid transformations of binary inorganic oxide systems were reviewed to identify those binary systems which have heats of transformation greater than 100 watt-hours per pound (793.7 joules per gram) and which have transformation temperatures in

---

*AFAPL-TR-75-92-Part 1, <u>Evaluation of Eutectic Fluoride Thermal Energy Storage Unit Compatibility</u>, October 1975.

the range of 538-760°C. These properties, the transformation temperature and the heat of transformation, together with the values for the thermal diffusivity of the solid phase and the density of the liquid phase were experimentally measured.

The compatibility of the inorganic oxides with Inconel, stainless steel, and refractory metal alloys was assessed by comparing the values for the Gibb's free energy of formation of the oxides from their elemental constituents. Test specimens of a binary inorganic oxide, $Li_2O-B_2O_3$, were sealed in an Inconel alloy container and these sealed containers were exposed to thermal environments between 538 and 760°C to confirm these evaluations.

2.1.1   Heat of Fusion

A survey was conducted of the values which have been published for the heat of fusion of pure inorganic oxides. The results of this survey are presented in Table 1. Values of 53 oxides of 32 elements are presented in this table. A total of nine of the pure oxides were identified which have values for the heat of fusion which is greater than 100 watt-hours per pound.

2.1.2   Melting Temperatures

The values for the melting temperature of the pure inorganic oxides which were surveyed are included in Table 1. None of the pure oxides which have a value for the heat of fusion greater than 100 watt-hours per pound (793.7 joules per gram) have a melting temperature in the desired range of 538 to 760°C.

2.1.3   Selected Binary Oxide Systems

The phase diagrams of binary inorganic oxide systems were reviewed to identify those liquid-solid transformations which are in the temperature range of 538 to 760°C. Five different types of liquid-solid transformations were observed among the inorganic systems which were reviewed. These types are; the

4

TABLE 1

HEAT OF FUSION AND MELTING TEMPERATURE
OF SELECTED SINGLE OXIDES

Oxide	Heat of Fusion		Melting Temp.		Ref
	kJ/g	watt-hr/lb	Deg C	Deg F	
ThO_2	4.6129	581.09	2952	5346	3
BeO	2.5258	318.18	2547	4617	1
Li_2O	(1.9603)	(246.93)	1570	2858	1
MgO	(1.9201)	(241.87)	2825	5117	1
Al_2O_3	1.1613	146.29	2042	3708	1
V O	0.9375	118.10	2077	3771	3
CaO	0.8953	112.78	2600	4712	3
TiO	(0.8512)	(107.23)	1750	3182	1
TiO_2	(0.8376)	(105.55)	1870	3398	1
V_2O_3	0.7816	98.46	1977	3591	3
Na_2O	0.7696	96.94	1132	2069	1
Ti_2O_3	(0.7681)	(96.77)	1839	3342	1
MnO	0.7668	96.59	1785	3245	2
Mn_3O_4	0.7131	89.83	1590	2894	3
ZrO_2	(0.7063)	(88.97)	2677	4581	1
VO_2	0.6861	86.42	(1545)	(2813)	2
SrO	0.6743	84.95	2460	4460	2
Ti_3O_5	(0.6172)	(77.76)	1774	3223	1
Fe_3O_4	0.5963	75.12	1597	2907	1
Cb_2O_5	0.4722	59.49	1460	2660	2
Y_2O_3	0.4632	58.36	2500	4532	4
Fe_9O	0.4549	57.31	1377	2511	1
Ta_2O_5	0.4545	57.25	1877	3411	3
GeO_2	0.4201	52.91	1116	2042	2
Cu_2O	0.3971	50.06	1236	2257	1
BaO	0.3761	47.38	1923	3493	3
V_2O_5	0.3589	45.21	670	1238	2
MoO_3	0.3372	42.48	801	1474	1
FeO	(0.3348)	(42.18)	(1377)	(2511)	1
WO_3	0.3167	39.89	1472	2682	1
B_2O_3	0.3160	39.81	450	842	1
ZnO	0.2298	28.95	1975	3587	4
WO_2	0.2229	28.08	1270	2318	3
SnO	0.1988	25.04	1042	1908	3

5

TABLE 1 (concluded)

| Oxide | Heat of Fusion | | Melting Temp. | | Ref |
	kJ/g	watt-hr/lb	Deg C	Deg F	
Sb_2O_3	0.1938	24.41	655	1206	3
Co_2	0.1803	22.71	-58	-72	1
N_2O_4	0.1592	20.06	-11	12	1
CrO_3	0.1577	19.87	198	388	3
TcO_7	0.1574	19.81	119	246	2
N_2O	0.1486	18.72	-91	-132	3
Re_2O_7	0.1322	16.65	296	565	2
SiO_2	0.1281	16.14	1423	2593	1
SO_2	0.1156	14.56	-76	-105	2
CrO_3	0.1156	14.56	2280	4136	3
PbO	0.1143	14.40	897	1647	1
ReO_3	0.0929	11.70	160	320	3
As_2O_3	0.0846	10.65	313	594	3
NO	0.0767	9.66	-164	-263	3
P_2O_3	0.0647	8.15	24	75	2
Bi_2O_3	0.0616	7.69	817	1503	3
Re_2O_8	0.0318	4.00	147	296	3
SO_3	0.0261	3.29	17	63	2

REFERENCES

1. JANAF Thermochemical Tables, 2nd Edition, Dow Chemical Company. Midland, Michigan.

2. Kubaschewski and Evans, Metallurgical Thermochemistry, 3rd Edition, Pergamon Press, New York, 1958.

3. Wicks and Block, Thermodynamic Properties of 65 ELEMENTS, Bureau of Mines Bulletin, 605, 1963.

4. Handbook of Materials Science, Volume 1: General Properties, CRC Press, Cleveland, Ohio, 1974.

eutectic, the congruent melting of an intermediate solid phase, and the peritectic, the syntectic, and the monotectic transformations. Although all of these liquid-solid transformations are reversible in the thermodynamic sense, only the first two types of liquid-solid transformations are reversible in a practical sense. The long times required to attain equilibrium on cooling of the other three types of liquid-solid transformations make their application to TES impractical.

The review of the phase equilibrium was limited to binary inorganic oxide systems in which at least one of the component oxides has a value for the heat of fusion which is greater than 100 watt-hours per pound (793.7 joules per gram).

The sixty binary systems which were reviewed are presented in Table 2. The liquid-solid transformation temperatures which have been reported in these systems are presented in Table 3. Seven of these binary systems have transformations in the required temperature interval.

The liquid-solid transformations which have been reported and presented in the binary phase diagrams of these seven systems are described in the following paragraphs. The data collected on the remaining fifty-three binary systems is presented in the Appendix.

$Li_2O-B_2O_3$

Eight compounds and two different eutectic transformations are depicted in the phase diagram of this system. The temperature-composition phase diagram is presented in Figure 1. The eutectic transformation at 650°C and 48 weight percent dilithium oxide is recommended for further study as a thermal energy storage material.

$Li_2O-Bi_2O_3$

Based on an investigation near the Bi_2O_3 rich component, an eutectic transformation at 690°C and at 11 mole percent

TABLE 2

BINARY INORGANIC OXIDE SYSTEMS WHICH WERE REVIEWED AS POTENTIAL CANDIDATES FOR THERMAL ENERGY STORAGE SYSTEMS

a. ThO_2
- $-B_2O_3$
- $-BeO$
- $-SiO_2$
- $-TiO_2$
- $-UO_2$
- $-Y_2O_3$
- $-ZrO_2$

b. BeO
- $-Al_2O_3$
- $-BaO$
- $-CaO$
- $-La_2O_3$
- $-MgO$
- $-SiO_2$
- $-SrO$
- $-ThO_2$
- $-TiO_2$
- $-UO_2$
- $-WO_3$
- $-Y_2O_3$
- $-Yb_2O_3$
- $-ZrO_2$

c. Li_2O
- $-Al_2O_3$
- $-B_2O_3$
- $-Bi_2O_3$
- $-Fe_2O_3$
- $-GeO$
- $-MnO$
- $-MoO_3$
- $-SiO_2$
- $-TiO_2$
- $-V_2O_5$
- $-WO_3$

d. MgO
- $-Al_2O_3$
- $-B_2O_3$
- $-BaO$
- $-BeO$
- $-Bi_2O_3$
- $-CO_2$
- $-CaO$
- $-CoO$
- $-Cr_2O_3$
- $-Cu_2O$
- $-FeO$
- $-Fe_2O_3$

d. MgO(cont.)
- $-GeO_2$
- $-H_2O$
- $-MnO$
- $-NiO$
- $-P_2O_5$
- $-PuO_2$
- $-SiO_2$
- $-SrO$
- $-Ta_2O_5$
- $-TiO_2$
- $-UO_2$
- $-V_2O_5$
- $-Y_2O_3$
- $-ZnO$
- $-ZrO_2$
- $-WO_3$

e. Al_2O_3
- $-B_2O_3$
- $-BaO$
- $-BeO$
- $-Bi_2O_3$
- $-CaO$
- $-CeO_2$
- $-Cr_2O_3$
- $-CuO$
- $-Hg_2O_3$

TABLE 3

TEMPERATURES AND COMPOSITIONS OF LIQUID-SOLID TRANSFORMATIONS OF BINARY INORGANIC OXIDES

System A B	Transformation Temp. (°C)	Type*	Compound A:B	Eutectic Weight%	Eutectic Mole%
$ThO_2 - B_2O_3$	1483	S	1:1		
	~1483	E			80-82 ThO_2
$ThO_2 - BeO_3$	2375	E			87 ThO_2
$ThO_2 - SiO_2$	1975	P	1:1		
	2000	M			
$ThO_2 - Al_2O_3$	1980	P	3:1		
	1870	C	1:1		
	1910	C	1:3		
	1835	E		25 BeO	
	1850	E		15 BeO	
	1890	E		6 BeO	
BeO - BaO	1284	P	1:3		
	1337	P	3:2		
	1430	P	3:1		
	1141	E		10 BeO	
BeO - CaO	1384	P	3:2		
	1384	E			38 BeO
$BeO - La_2O_3$	1514	P	1:1		
	1371	P	2:1		
	1371	E		12 BeO	
BeO - MgO	1855	E			57 BeO
$BeO - SiO_2$	(1670)	E		80 BeO	
BeO - SrO	1385	P	1:3		
	1306	P	1:1		
	1336	P	3:2		
	1380	P	4:1		
	1302	E		23 BeO	
$BeO - TiO_2$	1670	E		17 BeO	
$BeO - UO_2$	2175	E			70 BeO

* C-congruent melting, E-eutectic, M-monotectic, P-peritectic, S-syntectic.

TABLE 3 (Continued)

TEMPERATURES AND COMPOSITIONS OF LIQUID-SOLID TRANSFORMATIONS OF BINARY INORGANIC OXIDES

System A B	Transformation Temp. (°C)	Type*	Composition Compound A:B	Eutectic Weight%	Mole%
BeO - WO$_3$	1185	E			60 BeO
BeO - Y$_2$O$_3$	1580	E			65 BeO
BeO - Yb$_2$O$_3$	1720	E			65 BeO
BeO - ZrO$_2$	2145	E			68 BeO
Li$_2$O - Al$_2$O$_3$	1700	C	1:1		
	1950	C	6:1		
**Li$_2$O - B$_2$O$_3$	650	E		52 B$_2$O$_3$	
	832	E		73 B$_2$O$_3$	
	715	P	3:1		
	700	P	3:2		
	849	C	1:1		
	917	C	1:2		
	856	P	2:5		
	834	P	1:3		
	635	P	1:4		
Li$_2$O - Bi$_2$O$_3$	∿690	E			11 Li$_2$O
Li$_2$O - "Fe$_2$O$_3$"	1618	C	1:1		
	1510	E			40 Li$_2$O
Li$_2$O - GeO$_2$	1280	C	2:1		
	1120	C	3:2		
	1230	C	1:1		
	945	C	3:8		
	1030	C	1:7		
Li$_2$O - GeO$_2$	930	E		10 Li$_2$O	
	935	E		9 Li$_2$O	
	1025	E		3 Li$_2$O	
	1105	E		27 Li$_2$O	
	1115	E		32 Li$_2$O	

** Binary system recommended for further study.

TABLE 3 (Continued)

TEMPERATURES AND COMPOSITIONS OF LIQUID-SOLID
TRANSFORMATIONS OF BINARY INORGANIC
OXIDES

System		Transformation Temp. (°C)	Type*	Composition Compound A:B	Eutectic Weight%	Mole%
A	B					
Li_2O - MoO_3		705	C	1:1		
		530	P	1:2		
		550	P	1:3		
		565	P	1:4		
		525	E			26 Li_2O
Li_2O - SiO_2		1255	P	2:1		
		1201	C	1:1		
		1033	P	1:2		
		1024	E		46 Li_2O	
		1028	E		18 Li_2O	
Li_2O - TiO_2		1220	E		5 Li_2O	
		(1350)	C	1:3		
Li_2O - V_2O_5		621	P	2:7		
		601	P	2:5		
		620	C	1:1		
		560	E			40 Li_2O
Li_2O - WO_3		745	C	1:1		
		750	C	1:2		
		800	P	1:4		
		697	E			80 Li_2O
		745	E			45 Li_2O
MgO - Al_2O_3		2105	C	1:1		
		1995	E		46 MgO	
		1920	E			5 MgO
MgO - B_2O_3		988	P	1:1		
		1340	C	2:1		
		1366	C	3:1		
		1358	E		70 MgO	
		1313	E		56 MgO	
		1142	M			
MgO - BaO		1500	E			41 MgO
MgO - Bi_2O_3		785	E			20 MgO

TABLE 3 (Continued)

TEMPERATURES AND COMPOSITIONS OF LIQUID-SOLID TRANSFORMATIONS OF BINARY INORGANIC OXIDES

System A	B	Transformation Temp. (°C)	Type*	Compound A:B	Eutectic Weight%	Mole%
MgO	CaO	2370	E		35 MgO	
MgO	Cr$_2$O$_3$	2400	C	1:1		
		2350	(E)		37 MgO	
MgO	Cu$_2$O	1190	uncertain			20 MgO
MgO	Fe$_2$O$_3$	1725	P		10 MgO	
MgO	GeO$_2$	1700	C	1:1		
		1855	C	2:1		
		1495	P	4:1		
		1830	E			70 MgO
		1495	E			51 MgO
		1483	M			
MgO	P$_2$O$_5$	1857	C	3:1		
		1382	C	2:1		
		1165	C	1:1		
		1150	E		26 MgO	
		1282	E		58 MgO	
		1325	E		51 MgO	
MgO	PuO$_2$	2000	E			47 MgO
MgO	SiO$_2$	1890	C	2:1		
		1557	P	1:1		
		1695	E		31 MgO	
		1850	E		61 MgO	
		1695	M			
MgO	SrO	1950	(E)			45 MgO
MgO	Ta$_2$O$_5$	(1790)	C	1:1		
		1820	C	4:1		
		(1610)	E			20 MgO
		(1700)	E			70-75 MgO
MgO	TiO$_2$	1690	C	1:2		
		1680	P	1:1		
		1740	P	2:1		
		1600	E			55 MgO
		1610	E			80 MgO

12

TABLE 3 (Concluded)

TEMPERATURES AND COMPOSITIONS OF LIQUID-SOLID TRANSFORMATIONS OF BINARY INORGANIC OXIDES

System		Transformation Temp. (°C)	Type*	Composition Compound A:B	Eutectic Weight%	Mole%
A	B					
MgO - TiO$_2$		1652	C	1:2		
		1630	C	1:1		
		1732	C	2:1		
		1583	E			57 MgO
		1592	E			45 MgO
		1606	E			15 MgO
		1707	E			80 MgO
MgO - UO$_2$		1750	E			50 MgO
MgO - V$_2$O$_5$		756	P	1:1		
		917	P	2:1		
		1159	P	3:1		
		639	E			20 MgO
MgO - Y$_2$O$_3$		2300	C	3:1		
		1980	E			50 MgO
		2015	E			85 MgO
MgO - ZnO		1850	E		30 MgO	
MgO - ZrO$_2$		2050	E			50 MgO

13
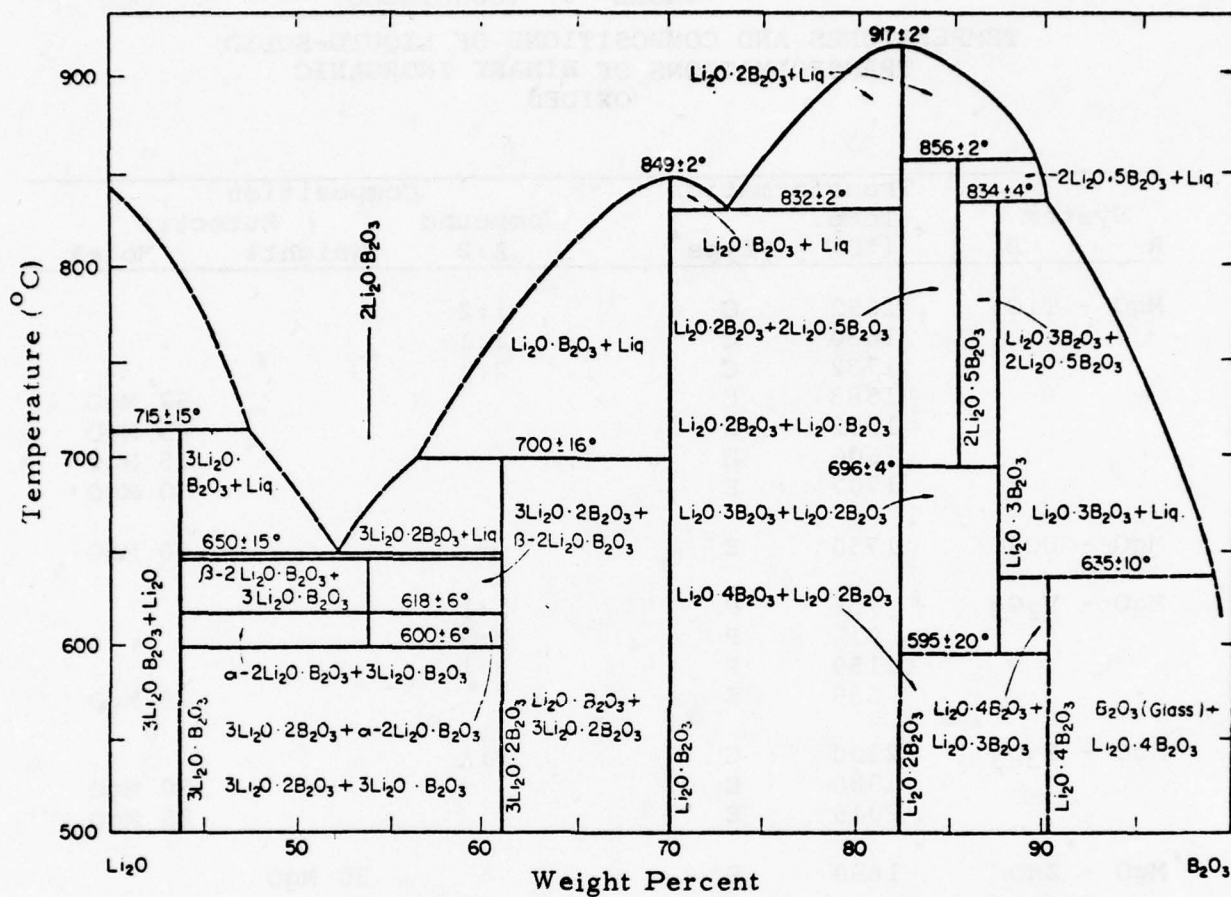
Figure 1. The Li$_2$O–B$_2$O$_3$ System. (Reference: B.S.R. Sastry and F.A. Hummel, Journal of the American Ceramic Society, 42(5)218(1959)).

14

dilithium oxide has been estimated and presented in the construction of the phase diagram in Figure 2.

Li_2O-MoO_3

The composition range between 0 and 50 mole percent dilithium oxide has been studied. Four compounds and one eutectic composition are reported in this range. Three of the four compounds have peritectic transformations in the range of 530°C to 575°C. The liquidus boundary at the composition $Li_2O \cdot MoO_3$ indicates a congruent melting compound at 705°C. The eutectic transformation occurs at 26 mole percent dilithium oxide and 525°C. This composition is presented in Figure 3.

$Li_2O-V_2O_5$

Three intermediate compounds are presented in the phase diagram in Figure 4. Two of the compounds undergo peritectic transformations at temperatures of 601°C and 621°C, respectively. The compound, $Li_2O \cdot V_2O_5$, melts congruently at a temperature of 620°C. An eutectic transformation is reported at 560°C and 40 mole percent dilithium oxide.

Li_2O-WO_3

Three compounds and two eutectics are reported in this system and presented in the phase diagram in Figure 5. The compound, $Li_2O \cdot WO_3$, melts congruently at 745°C, and the compound, $Li_2O \cdot 2 WO_3$, melts congruently at 750°C. The third compound undergoes a peritectic transformation at 800°C. The eutectic transformations which have been reported occur at 697°C and 40 mole percent dilithium oxide and 745°C and 22 mole percent dilithium oxide.

$MgO-V_2O_5$

Three peritectic compounds and one eutectic transformation are presented in the phase diagram in Figure 6. The eutectic transformation occurs at 639°C and 20 mole percent magnesia.
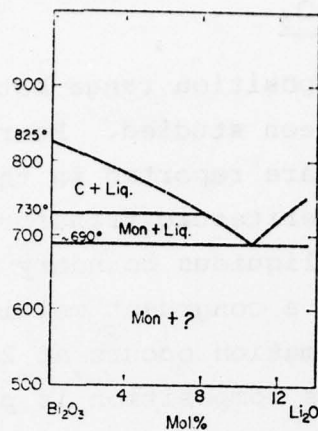
Figure 2.   The Li$_2$O-Bi$_2$O$_3$ System. (Reference: E.M. Levin and
R.S. Roth, J. Research Natl. Bur. Standards, 68A
[2] 198 (1964).)
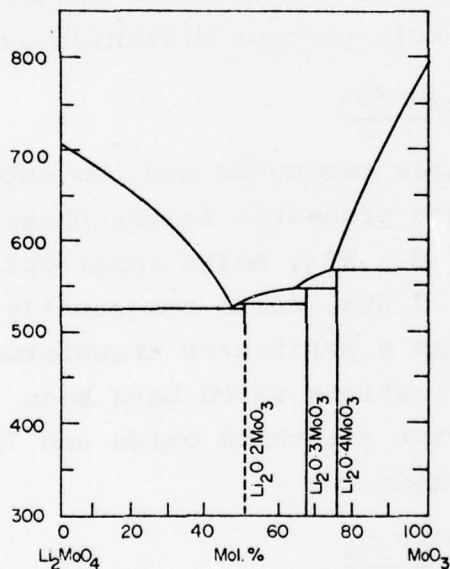
Figure 3.   The Li$_2$O-MoO$_3$ System. (Reference: F. Hoermann,
Z. Anorg. U. Allgem. Chem., 177, 154, (1928-1929).)
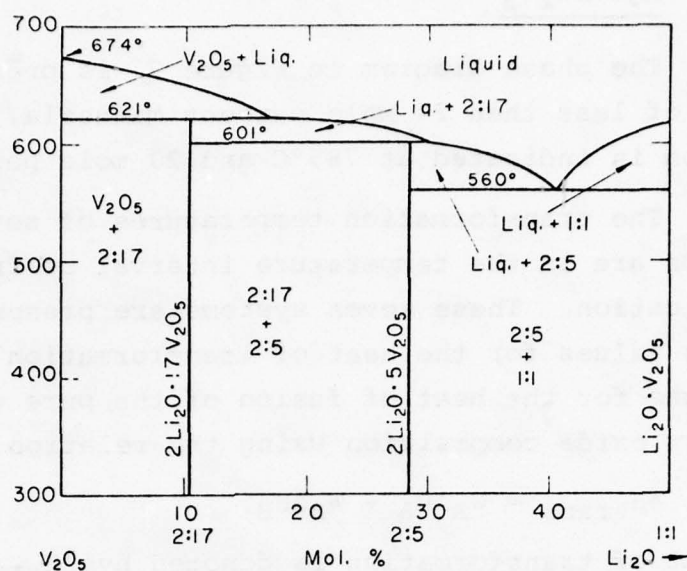
Figure 4. The Li$_2$O-V$_2$O$_5$ System. (Reference: A. Reisman and J. Mineo, J. Phys. Chem., 66, 1184 (1962).)
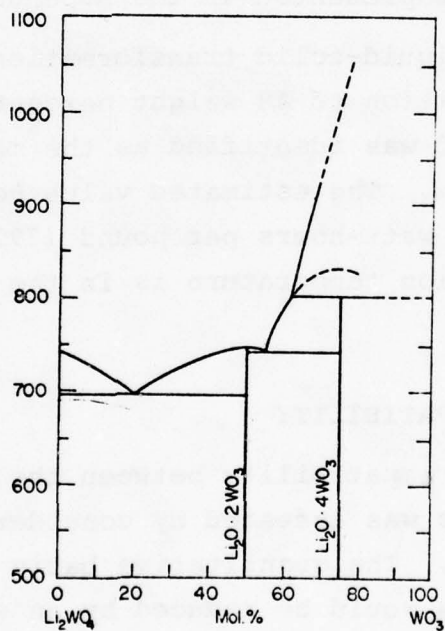
Figure 5. The Li$_2$O-WO$_3$ System. (Reference: F. Hoermann, Z. Anorg. U. Allgem. Chem., 177, 163 (1928-1929).)

$MgO-Bi_2O_3$

The phase diagram in Figure 7 is presented for compositions of less than 24 mole percent magnesia. An eutectic transformation is indicated at 785°C and 20 mole percent magnesia.

The transformation temperatures of seven of these binary systems are in the temperature interval of interest for the TES application. These seven systems are presented in Table 4. The values for the heat of transformation are estimated from the values for the heat of fusion of the pure components and the binary oxide composition using the relation:

$$\Delta H_{trans} = W_A \Delta H_A + W_B \Delta H_B,$$

where the heat of transformation is denoted by ΔH_{trans}, the heat of fusion of the pure inorganic oxides by ΔH_A and ΔH_B, and the weight fractions of the pure components are denoted by W_A and W_B. A detailed analysis of this method for estimating the heat of transformation is presented in the Appendix.

The liquid-solid transformation in the $Li_2O-B_2O_3$ located at a composition of 48 weight percent Li_2O and at a temperature of 650°C was identified as the most favorable inorganic oxide system. The estimated value heat of transformation is greater than 100 watt-hours per pound (793.7 joules per gram) and the transformation temperature is in the desired temperature interval.

2.2 CONTAINER COMPATIBILITY

The chemical compatibility between the inorganic oxides and container alloys was assessed by considering the oxidation-reduction reactions. The quantitative basis for judging whether the inorganic oxides would be reduced by an element of the container alloy is by comparing the values for the Gibb's free energy of formation of the oxides. Thus, the direction of the oxidation-reduction reaction specified by the equation,

$$Li_2O + Ni \rightleftarrows 2 LI + NiO,$$

18
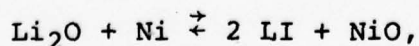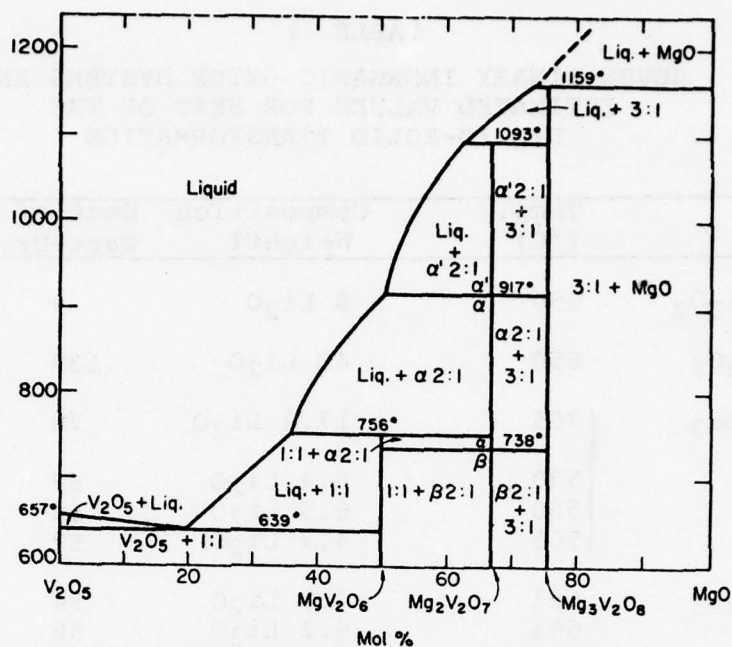
Figure 6.   The MgO-V$_2$O$_5$ System. (Reference: R. Wollast and A. Tozairt, Silicates Ind., 34(2) 42 (1969).)
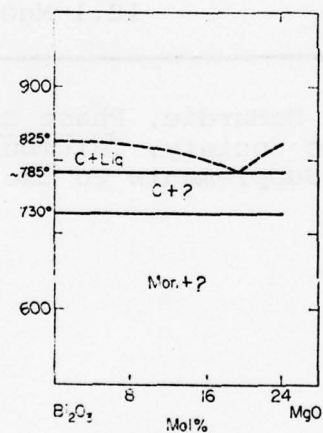
Figure   7.   The MgO-Bi$_2$O$_3$ System. (Reference: E.M. Levin and R.S. Roth, J. Research Natl. Bur. Standards, 68A(2) 199 (1964).

19

TABLE 4

SEVEN BINARY INORGANIC OXIDE SYSTEMS AND ESTIMATED VALUES FOR HEAT OF THE LIQUID-SOLID TRANSFORMATION

System*	Temp. (°C)	Composition Weight%	Heat of Transformation Watt-Hr./lb.	J/g
1. $Li_2O-Bi_2O_3$	690	8 Li_2O	9	71
2. $Li_2O-B_2O_3$	650	48 Li_2O	139	1103
3. Li_2O-MoO_3	705	17.2 Li_2O	78	619
	530	9.4 Li_2O	62	492
	550	6.5 Li_2O	56	444
	565	4.9 Li_2O	52	413
4. $Li_2O-V_2O_5$	621	4.5 Li_2O	54	429
	601	6.2 Li_2O	58	460
	620	14.1 Li_2O	74	587
5. Li_2O-WO_3	745	11.4 Li_2O	63	500
6. $MgO-Bi_2O_3$	785	2.1 MgO	13	103
7. $MgO-V_2O_5$	750	18.1 MgO	81	643

*Levin, Robbins, and McMurdie, Phase Diagrams for Ceramists, The American Ceramic Society, Columbus, Ohio, 1964. (See also 1969 and 1975 Supplements to the Basic publication.)

20

can be determined by comparing the values for the free energy
of formation of the two oxides. If the dilithium oxide has a
larger value than the nickel oxide for the free energy of forma-
tion, then the chemical equilibrium will lie on the left-hand
side of the equation. The values for the free energy of forma-
tion of selected inorganic oxides is presented in Table 5. The
oxides in this table include all of the high performance materials
identified in Table 1. In addition the oxides of the alloying
elements of the Inconel and stainless steel alloys are included
in this compilation. These alloying elements are presented
in Table 6. Not all of the stainless steel or Inconel alloys
use all of the alloying elements.

As an example of the application of this table, consider
the oxidation reduction behavior which can be expected to occur
between the inorganic eutectic oxides in the $Li_2O-B_2O_3$ system
and a container fabricated from either a stainless steel or an
Inconel alloy. The values for the free energy of the Li_2O com-
ponent is more stable than that of any of the oxides of the
alloying elements of either stainless steel or Inconel with the
single exception of magnesium. The comparison for the B_2O_3 com-
ponent shows that the alloying elements, aluminum, magnesium
titanium, and silicon all have oxides which are more stable than
the B_2O_3. Thus, those stainless steel or Inconel alloys which
contain these alloying elements should be avoided for container
materials.

Since other reactions are possible, such as solubility of
one or more of the alloying components in the inorganic oxide
eutectic melt, the chemical compatibility was experimentally
verified.

21

TABLE 5

VALUES FOR THE FREE ENERGY OF FORMATION OF SELECTED INORGANIC OXIDES (REF: BUREAU OF MINES BULLETIN 542)
$-\Delta F°$ PER OXYGEN ATOM IN KILOCALORIES

Oxide	25.16°C (77.288°F)	527°C (980.6°F)	727°C (1340.6°F)
1. ThO_2	139.6	127.9	123.3
2. MgO	136.1	123.1	117.7
3. BeO	136.1	124.3	119.6
4. Li_2O	133.8	117.3	110.2
5. Al_2O_3	125.8	113.2	108.2
6. TiO	116.9	105.5	101.1
7. SiO_2	98.4	87.6	83.4
8. B_2O_3	95.5	85.2	81.7
9. VO	93.5	83.0	79.0
10. Ta_2O_5	91.3	80.8	76.7
11. Nb_2O_4	88.6	77.9	73.7
12. MnO	86.7	78.0	74.6
13. Cr_2O_3	84.4	73.8	69.7
14. V_2O_5	68.3	58.1	54.4
15. P_4O_{10}	65.4	54.3	50.2
16. Fe_3O_4	60.8	51.0	47.5
17. MoO_2	60.7	52.0	48.5
18. CoO	51.6	42.5	38.8
19. NiO	50.6	39.5	35.1
20. CO_2	47.1	47.3	47.3
21. SO_2	35.9	--	--
22. Cu_2O	35.0	26.5	23.3
23. SeO_2	20.8	12.8	11.8

22

TABLE 6

ELEMENTAL ALLOYING CONSTITUENTS OF STAINLESS
STEEL AND INCONEL ALLOYS

iron	molybdenum
nickel	titanium
chromium	sulfur
aluminum	copper
carbon	magnesium
manganese	columbium
silicon	tantalum
cobalt	phosphorus
selenium	

SECTION III
THERMOPHYSICAL PROPERTIES

Selected thermophysical properties of eutectic compositions in the $Li_2O-B_2O_3$ system, the $LiF-MgF_2$, the $LiF-MgF_2-KF$, and the $LiF-MgF_2-NaF$ systems have been experimentally determined. The thermophysical properties which were measured were the heat of the liquid-solid transformation, the temperature of the liquid-solid transformation, the density of the liquid, and the thermal diffusivity-thermal conductivity of the solid phases as a function of temperature.

3.1 CALORIMETRIC EXPERIMENT

The heat of the liquid-solid transformation was determined from the difference between the values of the heat content of the liquid and solid phases at the eutectic temperature. The experimental arrangement used for the determination of the values of the heat content as a function of temperature is presented in Figure 8. The specimen, 2, was brought to thermal equilibrium in the furnace, 1. The temperature of the specimen was measured with a chromel-alumel thermocouple, 3, and displayed on an Omega type 2809 Digital Thermometer. After reaching thermal equilibrium in the furnace, the specimen was physically dropped into the copper block, 6. The heat energy transferred by the specimen to the copper block caused a temperature rise of the block. The temperature rise of the copper block was detected by a 12 junction iron-constantine thermopile, 10. The cold junction of each thermocouple of the thermopile was immersed in an ice-water bath. The electromotive force generated by the thermopile was displayed on a Honeywell Electronik 194 recorder. Thus, the deflection of the recording potentiometer was proportional to the temperature rise of the copper block. The copper block was mounted within a water tight container, and the entire subassembly was immersed in an isothermal bath, 8. The cavity in the copper block was fitted with a cover which was closed

24
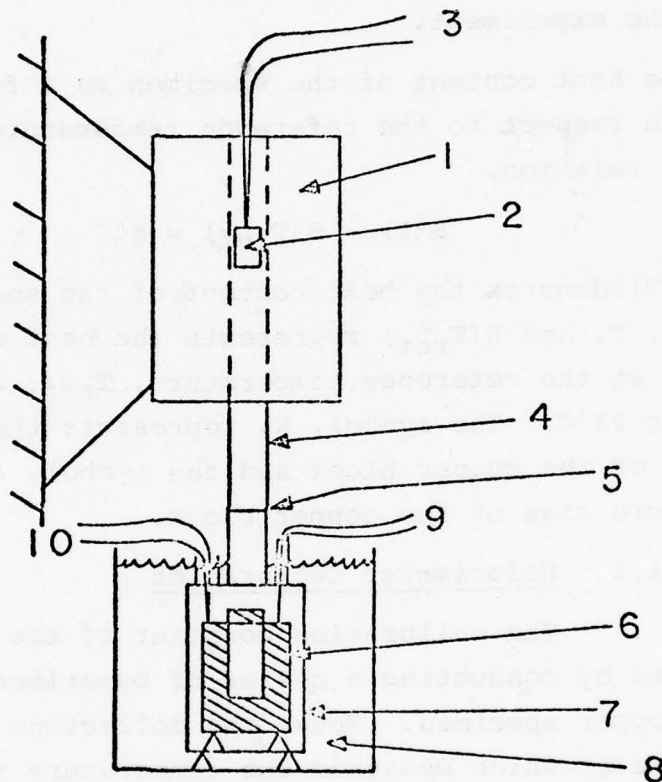
Figure 8. Experimental Arrangement for Measuring
the Value for the Heat of Fusion.

immediately after the specimen had been dropped in order to minimize heat losses as the specimen cooled. The furnace and the calorimeter subassemblies were connected with an Inconel alloy tube, 4, which contained a gate, 5, which was only opened when the specimen was dropped. The purpose of the gate was to prevent thermal radiation from reaching the copper block from the furnace. An argon atmosphere was maintained within the furnace and the calorimeter subassemblies to prevent oxidation of the specimen during the experiment.

The heat content of the specimen as a function of temperature with respect to the reference temperature was determined from the relation,

$$H(T) - H(T_{ref}) = K\Delta T \tag{1}$$

where H(T) denotes the heat content of the specimen at the temperature, T, and $H(T_{ref})$ represents the heat content of the specimen at the reference temperature, T_{ref}, which was maintained at 25°C. The symbol, K, represents the calibration constant of the copper block and the symbol, ΔT, denotes the temperature rise of the copper block.

3.1.1 Calorimeter Calibration

The calibration constant of the copper block was determined by conducting a series of experimental measurements with a copper specimen. Thus, the deflection of the recording potentiometer which measured the temperature rise of the copper block was correlated with a specimen whose values for the heat content as a function of temperature are known. The values for the heat content of copper have been tabulated as a function of temperature by Hultgren et al.[*] The temperature of the copper block was measured for at least twenty minutes before and after each experimental determination. The slight changes which were

---

[*]Hultgren, et al., Selected Values of Thermodynamic Properties of Metals and Alloys, American Society for Metals, Metals Park, Ohio, 1973.

26

observed in the temperature during these time intervals were
utilized to obtain a corrected value for the temperature rise
due to the heat transfer of the specimen. The experimental data
for the calibration determinations are presented in Table 7A.
The temperature of the copper specimen in the furnace at the
time it was dropped into the calorimeter subassembly is presented
in column 1, the deflection of the recording potentiometer which
measured the temperature changes in the copper block are pre-
sented in column 2, and the calibration constant for each datum
point is presented in column 3.

An additional 14 experimental measurements were con-
ducted on the copper specimen in the temperature interval of
481.5°C to 951°C. The data from these additional measurements
are presented in Table 7B. The values of the copper calibra-
tion experiments as determined from these additional measurements
are 8.3 percent below the values which were obtained by extra-
polation of the data presented in Table 7A into the tempera-
ture interval of 500°C to 950°C. This difference is attributed
in part to the heat energy which is lost from the copper specimen
in its free fall from the furnace to the calorimeter. As the
temperature of the furnace increases the amount of energy radiated
during the free fall increases with an apparent decrease in the
calibration constant. Those experiments for which the measured
deflection is greater than 10 centimeters were calculated with
this additional copper calibration data.

3.1.2   Heat Content of Type 303 Stainless Steel

The values for the heat content of type 303 stain-
less steel were determined as a function of temperature over the
temperature interval of 39°C to 781°C. These values were cal-
culated from experimental data with the aid of equation 1.
The experimental data for the stainless steel determinations are
presented in Table 8. The temperatures of the stainless steel
which were measured at the time it was dropped from the furnace
are presented in column 1. The values for the deflection, in

27

TABLE 7

DETERMINATION OF THE CALIBRATION CONSTANT, K, OF EQUATION 1

A. Copper Specimen Temperatures Between 67°C and 418°C
   Copper Mass: 27.09 grams

Specimen Temperature (°C)	Potentiometer Deflection (cm)*	Calibration Constant (joules/cm)
67	0.794	548.2
98	1.429	518.5
111	1.707	513.5
117	1.905	511.8
159	2.857	504.7
180	3.254	503.0
207	3.929	501.8
222	4.286	501.8
243	4.604	501.4
270	5.398	501.8
288	5.753	501.8
300	6.191	502.2
332	6.548	503.0
338	6.826	503.0
352	7.064	503.5
364	7.302	503.9
387	7.897	504.7
389	7.977	504.7
418	8.334	506.0

*One centimeter of deflection of the recording potentiometer is
equal to a temperature rise of the copper block of 0.1239°C
at 25°C.

28

TABLE 7 (concluded)

DETERMINATION OF THE CALIBRATION CONSTANT, K, OF EQUATION [1]

B. Copper Specimen Temperatures Between 482°C and 951°C
Copper Mass: 26.64 grams

Specimen Temperature (°C)	Potentiometer Deflection (cm)*	Calibration Constant (joules/cm)
482	10.774	469.6
515	11.597	470.0
645	14.790	472.3
668	15.355	473.0
726	16.767	475.1
728	16.816	475.2
773	17.933	477.0
785	18.228	477.5
821	19.112	479.1
931	21.814	484.4
951	22.305	485.4

29

TABLE 8

EXPERIMENTAL DATA FOR THE DETERMINATION OF THE HEAT
CONTENT OF TYPE 303 STAINLESS STEEL

Specimen Temperature (°C)	Potentiometer Deflection (cm)	Mass (grams)	Heat Content (joules/gram)
39	0.238	10.56	13.85
103	0.794	10.56	41.26
158	1.389	10.56	68.55
222	2.183	10.56	105.17
254	2.064	8.54	123.21
254	1.864	9.29	102.74
300	2.937	10.55	140.36
344	3.016	9.29	163.59
346	2.699	8.54	159.70
388	4.128	10.55	192.28
420	4.445	10.54	211.51
476	5.318	10.55	252.90
521	4.961	9.29	267.88
573	6.231	10.55	296.72
646	6.426	9.29	347.65
693	7.818	10.55	373.97
749	7.381	9.29	400.46
781	7.858	9.29	426.91

centimeters, of the recording potentiometer which measured the temperature rise of the copper block are presented in column 2. Since all of the experimental potentiometer deflections are less than eight centimeters, the values for the calibration were taken from the data presented in Table 7A. These values include the corrections for the slight temperature drifts measured before and after the specimens were dropped. The mass of the stainless steel specimen is presented in column 3, and the values for the heat content of the stainless steel are presented in column 4. These values of the heat content as a function of temperature were fitted by the method of least squares to a linear equation. The analytical relation which was obtained for the heat content of type 303 stainless steel is,

$$H(T)-H(T_{ref}) = -23.65+0.5666T \text{ joules per gram } 39°C \leqslant T \leqslant 781°C \quad (2)$$

where the symbols, $H(T)$ and $H(T_{ref})$, denote the heat content of stainless steel at the temperature, T, and at the reference temperature, 23.9°C.

3.2   HEAT CONTENT OF THE EUTECTIC FLUORIDE SPECIMENS

The values for the heat content of compositions in the $LiF-MgF_2$ and the $LiF-MgF_2-KF$ system were measured as a function of temperature. The compositions of the inorganic fluoride specimens are presented in Table 9. The liquid-solid transformation temperatures of these compositions were measured to assist in the determination of the heats of the liquid-solid transformation.

3.2.1   Differential Thermal Analysis

The liquid-solid transformation temperature was measured in a Differential Thermal Analyzer. The temperature at which thermal events were observed are presented in Table 10. Two complete heating and cooling cycles were performed on the specimen. Two thermal events were observed on each heating cycle and three thermal events were observed on each cooling

31

TABLE 9

A. COMPOSITION OF THE LiF-MgF$_2$-KF EUTECTIC SPECIMEN

Component	Weight Percent
LiF	63.5
MgF$_2$	30.5
KF	6

B. COMPOSITION OF THE LiF-MgF$_2$ EUTECTIC SPECIMEN

LiF	68
MgF$_2$	32

TABLE 10

TEMPERATURES AT WHICH THERMAL EVENTS WERE OBSERVED

Heating Cycle	Cooling Cycle
A. LiF-MgF$_2$-KF	
1a. 630°C (very weak) 708°C (strong)	1b. 605°C (very weak) 703°C (strong) 714°C (weak)
2a. 635°C (very weak) 708°C (strong)	2b. 605°C (very weak) 702°C (strong) 714°C (weak)
B. Li$_2$O-B$_2$O$_3$	
1a. 650°C (strong)	1b. 625°C (strong)
C. LiF-MgF$_2$	
1a. 725°C (strong)	1b. 735°C (weak) 722°C (strong)

cycle. The major event which was observed was the eutectic transformation. The value for the eutectic transformation temperature is 705 ± 2°C. The thermal event at 714°C which was observed only on the cooling cycles is attributed to the precipitation of a pro-eutectic constituent from the liquid phase. The thermal event which was observed in the temperature interval 605°C to 630°C is attributed to a solid state transformation. Although the type of this solid-state transformation has not been positively identified, it is most probably related to the precipitation-solution reaction to be expected as the solvus boundary is transited. The trace from the DTA experiment indicated that the energy involved in this reaction is on the order of two percent of the energy of the liquid-solid transformation.

3.2.2   Eutectic Fluoride Experimental Data

The LiF-MgF$_2$-KF specimens were contained in a Type 303 stainless steel container. The values of the heat content of these capsules were measured as a function of temperature over the interval of 165°C to 755°C. The values for the heat content of the stainless steel containers were subtracted from the total experimentally observed quantities to determine the heat content of the inorganic fluoride specimen. The experimental data for these measurements are presented in Table 11A. The temperature of the specimen at the time it was dropped from the furnace into the calorimeter is presented in column 1. The temperature rise of the copper block as measured in centimeters of deflection of the recording potentiometer is listed in column 2. In columns 3 and 4 are the values for the mass of the fluoride specimen and the stainless steel container, and in column 5 are the values for the content of the fluoride composition. The values for the heat content were fitted as a function of temperature for the solid and liquid phases of the fluoride specimen by the method of least squares to a first order polynomial. The resulting analytical expressions are as follows:

33

a) solid-H(T)-H(T_{ref})= -265.2+1.8179T joules per gram,

$$389°C \leq T \leq 681°C \tag{3}$$

b) liquid-H_T-H(T_{ref})= 1495.4+0.3896T joules per gram,

$$715°C \leq T \leq 755°C \tag{4}$$

The reference temperature for these experiments was 23.9°C. The value for the heat of the liquid-solid transformation which was determined from the difference between these two expressions at the eutectic transformation temperature, is 753.6 joules per gram.

The LiF-MgF$_2$ specimen was contained in a Type 303 stainless steel container. The values of the heat content were measured over the temperature interval from 463°C to 825°C. The values for the heat content of the stainless steel container were subtracted from the total experimentally observed quantities to determine the heat content of the eutectic fluoride specimen. The experimental data for these measurements are presented in Table 11B. The values for the heat content for the solid and liquid phases were fitted as a function of temperature to a linear equation by the method of least squares. The resulting analytical expressions are as follows:

a) solid- H(T)-H(T_{ref}) = -719.6 + 2.7127T

$$463°C \leq T \leq 724°C \tag{5}$$

b) liquid- H(T)-H(T_{ref}) = 97.31 + 2.3168T

$$724°C \leq T \leq 825°C \tag{6}$$

The reference temperature for these experiments was 23.9°C. The value for the heat of the liquid-solid transformation at the eutectic transformation temperature, 724°C, is 530.3 joules per gram.

3.2.3 Experimental Data on the Li$_2$O-B$_2$O$_3$ Specimen

The eutectic composition in the Li$_2$O-B$_2$O$_3$ system at 52 weight percent B$_2$O$_3$ was prepared by combining measured amounts of B$_2$O$_3$ and Li$_2$O. This specimen was heated to 700°C and held for 30 minutes at this temperature. The specimen was cooled to room temperature and a sample was taken for a Differential Thermal Analysis measurement. A single thermal event was

34

TABLE 11A

EXPERIMENTAL DATA FOR THE DETERMINATION OF THE HEAT CONTENT OF THE LiF-MgF$_2$-KF SPECIMEN

| Specimen Temperature (°C) | Potentiometer Deflection (cm) | Mass | | Heat Content (joules/gm) |
		Fluoride (grams)	Stainless Steel (grams)	
165	2.461	8.54	5.46	115.5
276	6.350	9.29	6.95	285.1
341	7.144	8.54	6.95	314.5
389	10.636	9.29	6.95	476.8
408	10.478	9.29	6.95	452.9
435	11.192	9.29	6.95	483.2
436	9.604	8.54	5.46	504.1
474	10.676	8.54	5.46	566.2
476	13.256	9.29	6.95	596.9
488	11.351	8.53	5.46	614.1
537	12.422	8.54	5.46	666.6
539	14.764	9.29	6.95	656.6
559	15.081	9.29	6.95	664.3
562	14.049	8.54	5.46	778.9
591	16.113	9.29	6.95	713.0
598	13.970	8.53	5.46	751.6
622	16.193	8.53	5.46	928.6
636	20.082	9.29	6.95	960.4
644	17.145	8.53	5.46	994.7
681	18.574	8.53	5.46	1090.7
720	26.789	7.06	6.00	1733.8
723	28.178	7.06	6.00	1850.2
733	19.249	6.87	3.81	1740.6
739	26.392	9.15	5.31	1760.9
740	26.988	9.21	5.31	1812.5
754	26.194	10.29	5.04	1734.9
755	20.241	6.87	3.81	1846.6

35

TABLE 11B

EXPERIMENTAL DATA FOR THE DETERMINATION OF THE
HEAT CONTENT OF THE LiF-MgF$_2$ SPECIMEN

Mass: Fluoride - 4.6256 grams
       Stainless Steel - 8.7201 grams

Specimen Temperature (°C)	Potentiometer Deflection (cm)	Heat Content (Joules/gram)
463	10.30	595.5
483	10.57	601.3
534	12.14	708.4
538	12.29	719.9
576	13.78	834.5
602	14.83	912.4
605	13.83	808.3
644	16.45	1044.4
663	17.15	1099.9
681	17.82	1154.1
699	18.47	1206.0
741	24.19	1802.7
741	24.36	1830.7
771	25.32	1910.1
773	24.86	1854.2
783	25.42	1909.0
825	26.62	2004.8
825	26.72	2017.3

observed on the heating and cooling cycles. The liquid-solid transformation on the heating cycle occurred at a temperature of 650°C. On the cooling cycle the liquid phase was observed to supercool to a temperature of 595°C before the solid phase was nucleated. Since the temperature measured for a liquid-solid transformation on the heating cycle is a more reliable indicator of the transformation temperature the value of 650°C was adopted. The DTA results are presented in Table 10.

The measurements of the heat content of the Li_2O-B_2O_3 specimen contained in sealed 303 stainless steel capsule were conducted over a temperature interval of 535°C to 788°C. The data for these measurements are presented in Table 12. The analysis of these data shows that the discontinuity associated with the heat of the liquid-solid transformation occurs at a temperature greater than 627°C and less than 652°C. The values for the heat content as a function of temperature were fitted for the liquid and solid phases to linear equations by the method of least squares. The resulting analytical expressions for the heat content are as follows:

a) solid-$H(T)-H(T_{ref}) = -3040.2 + 15.293T$ joules, for
$$535°C \leqslant T \leqslant 605°C \qquad (7)$$

b) liquid-$H(T)-H(T_{ref}) = -630.96 + 13.969T$ joules, for
$$652°C \leqslant T \leqslant 788°C \qquad (8)$$

The reference temperature for these experiments was 23.9°C. The value for the heat of the liquid-solid transformation which was determined from the difference between these two expressions at 650°C is 414.1 joules per gram.

3.2.4 Accuracy of the Measurement of the Heat of Fusion

The accuracy of the drop calorimetric technique for measurement of the heat content of a liquid or a solid phase depends on the control of the possible systematic experimental errors. The most common sources for systematic errors in this experiment are:

37

TABLE 12

EXPERIMENTAL DATA FOR THE DETERMINATION OF THE HEAT CONTENT OF THE $Li_2O-B_2O_3$ SPECIMEN

Specimen Temperature (°C)	Potentiometer Deflection (cm)	Heat Content* (joules)
535	11.19	5086.5
539	11.55	5251.4
546	11.67	5306.0
551	11.59	5269.6
555	11.75	5342.3
556	11.99	5451.4
558	12.38	5628.7
565	12.30	5592.3
571	12.46	5665.1
573	12.46	5665.1
577	13.02	5919.6
581	12.90	5865.1
588	13.10	5956.0
591	13.41	6096.9
600	13.57	6169.6
616	13.81	6278.7
609	13.97	6351.5
624	14.09	6406.0
627	14.29	6496.9
605	13.84	6291.0
652	18.14	8246.9
664	19.41	8824.2
666	19.53	8878.8
675	18.49	8406.0
675	20.00	9092.4
698	19.85	9024.2
704	20.24	9201.5
715	20.48	9310.6
716	22.39	10178.8
717	19.85	9024.2
720	20.40	9274.2
725	20.88	9492.4
730	20.48	9310.6
742	21.35	9706.1
742	21.63	9833.3
750	21.91	9960.6
755	21.07	9578.8
756	22.15	10069.7
765	21.67	9851.5
774	22.94	10428.8
788	22.86	10392.4

*The Mass of the $Li_2O-B_2O_3$ specimen was 3.74 grams.

The Mass of the stainless steel container was 8.91 grams.

38

1. Characterization of the initial and final states of the specimen,

2. Heat energy losses from the specimen during the drop from the furnace to the copper block,

3. Measurement of the calibration constant of the copper block, and

4. Determination of the temperature rise of the copper block due to the specimen during the heat transfer period.

The first possible error was investigated by comparing X-ray diffraction patterns of specimens which had been cycled back and forth through the liquid-solid transformation. In all cases the same solid phases were found to be present. For the measurements on the liquid phase the specimens were heated to 50°C above their melting point and held for 30 minutes and then equilibrated with the furnace cavity prior to the drop into the copper block.

The heat energy losses were minimized by dropping the empty container over the same temperature as the filled container. The heat content of the empty container varied continuously with the temperature from which it was dropped; whereas the filled container exhibited a discontinuity in the value for the heat content at the temperature of the liquid-solid transformation. The heat losses during the drop of the filled container should be approximately the same as the empty container and thus they tend to cancel.

The error in the calibration constant was minimized by dropping a copper specimen whose heat content as a function of temperature has been well established. The temperature rise of this copper block during these tests was adjusted to match those of the experiments of the fluoride and oxide specimens.

The error in measuring the temperature rise of the copper block which is due to the heat transfer of the specimen

39

was minimized by measuring the very slight drift in the temperature of the copper block immediately before and after each experiment. These temperature drifts were used to correct the temperature rise due to the heat transfer of the specimen. Any experiments in which irregularities were observed were discarded.

The value of the heat content measured by this experiment for the LiF-MgF$_2$-KF specimen was compared to the sum of the values for the heat content of the individual components which have been reported in the Janaf Thermochemical Tables. The two sets of values differed by four percent. Consequently, an overall accuracy of four percent was assigned to the value determined to the heat of the liquid-solid transformation.

3.3 THERMAL DIFFUSIVITY

The values for the thermal diffusivity were measured for the eutectic compositions of the LiO$_2$-B$_2$O$_3$, LiF-MgF$_2$-KF, and the LiF-MgF$_2$-NaF systems as a function of temperature using the flash technique.* This technique consists of generating a pulse of radiant energy, absorbing the energy pulse on one surface of a flat specimen, and measuring the temperature rise of the opposite surface as a function of time. The value for the thermal diffusivity is determined from an analysis of the experimental time-temperature rise plot. Carslaw and Jaeger** formulated the one-dimensional heat flow equation which describes this experiment.

Under the conditions that a heat pulse, Q, is uniformly absorbed in a depth, g, on the surface of an opaque insulated solid of uniform thickness, and where the time duration of the heat pulse is small compared to the transit time, then the ratio

---

* W.J. Parker, et al., "Flash Method of Determining Thermal Diffusivity Heat Capacity, and Thermal Conductivity," J. Appl. Phys., 32(9), 1679-1687 (1961).

**W.S. Carslaw and J.C. Jaeger, Conduction of Heat In Solids, 2nd Edition, Oxford Press, New York, New York, 1959.

of the temperature rise of the back surface of the specimen to the maximum temperature rise is given by,

$$\frac{T(\ell,t)}{T_{max}} = 1 + 2 \sum_{n=1}^{d} (-1)^n \exp\left(\frac{-n^2\pi^2\alpha t}{\ell^2}\right) \tag{9}$$

where the symbols ℓ, α, and t, are, respectively, the thickness of the specimen, the thermal diffusivity, and the time. The solution for this expression for,

$$\frac{T(\ell,t)}{T_{max}} = 1/2, \tag{10}$$

yields a simple relation among the thermal conductivity, the thermal diffusivity, and the time interval required for the back surface temperature to rise to one-half of its maximum value. The relation among these values is,

$$\alpha = \frac{0.139 \; \ell^2}{\tau_{1/2}} \tag{11}$$

The radiant energy pulse was generated by a power supply which triggered a flash tube. The pulse is impinged on the surface of the specimen and simultaneously triggers the circuit to mark the time base for the experiment. The specimens are mounted in a spring-loaded fixture which is thermally insulated to minimize heat losses. The back surface temperature response of the specimen is sensed with a chromel-constantan thermocouple. The EMF output of this thermocouple is amplified and displayed on a monitor oscilloscope and recorded on the waveform recorder. A waveform recorder provides digital storage of the high speed transient electrical signal for subsequent playback at a rate compatible with the writing speed of a conventional x-time recorder.

The measurements at elevated temperature were obtained by heating the specimen in a wire-wound resistance furnace. The temperature of the specimen was measured by a separate thermocouple. The front surface of the specimen was coated with a dry graphitic film lubricant to prevent radiative coupling of the radiant energy and the back surface thermocouple.

41

This experimental technique has been evaluated[*] by comparing the values for thermal diffusivity of several materials as determined in this experiment to the values which have been compiled in the Thermophysical Properties Research Center Data Book. The maximum difference between these two sets of thermal diffusivity data over the temperature interval of -65°C to 220°C was less than 5 percent.

3.3.1 Experimental Results

A typical plot of the back surface temperature rise of the specimen is presented in Figure 9. The experimental results for the thermal diffusivities of the four different eutectic compositions, are presented in Table 13.

3.4 DENSITY MEASUREMENTS

The value for the density of the liquid phase of the eutectic composition in the Li_2O-B_2O_3 at 48 weight percent Li_2O was measured by an adaptation of the maximum bubble pressure method.[**] In this experiment a stainless steel capillary tube is immersed in the liquid phase and inert gas is bubbled through the liquid. The pressure of the inert gas, P, of the bubble as it forms on the end of the capillary is related to the surface tension of the liquid, δ, the radius of the bubble, r, the immersion depth of the capillary tube below the surface of the liquid, h, and the densities of the liquid and the inert gas

[*]Thermal, Electrical, and Physical Property Measurements of Laser Window Materials, AFML-TR-75-28, April, 1975.

[**]Kingery, W.D., Property Measurements at High Temperatures, John Wiley & Sons, Inc., New York, New York, 1959.

[**]Greenaway, H.T., The Surface Tension and Density of Lead-Antimony and Cadmium Antimony Alloys, Journal of the Institute of Metals, 74, 133(1947).

[**]Hogness, T.R., The Surface Tensions and Densities of Liquid Mercury, Cadmium, Zinc, Lead, Tin, and Bismuth, Journal of the American Chemical Society, 43, 1621(1921).

TEMPERATURE RISE (20 μV/in)

TIME (0.25 sec/in)

LiF — MgF₂ — NaF
SPECIMEN 2
ℓ = .2212 cm

HEAT PULSE
INITIATION

ΔT

.5 ΔT

$t_{1/2}$

1 in
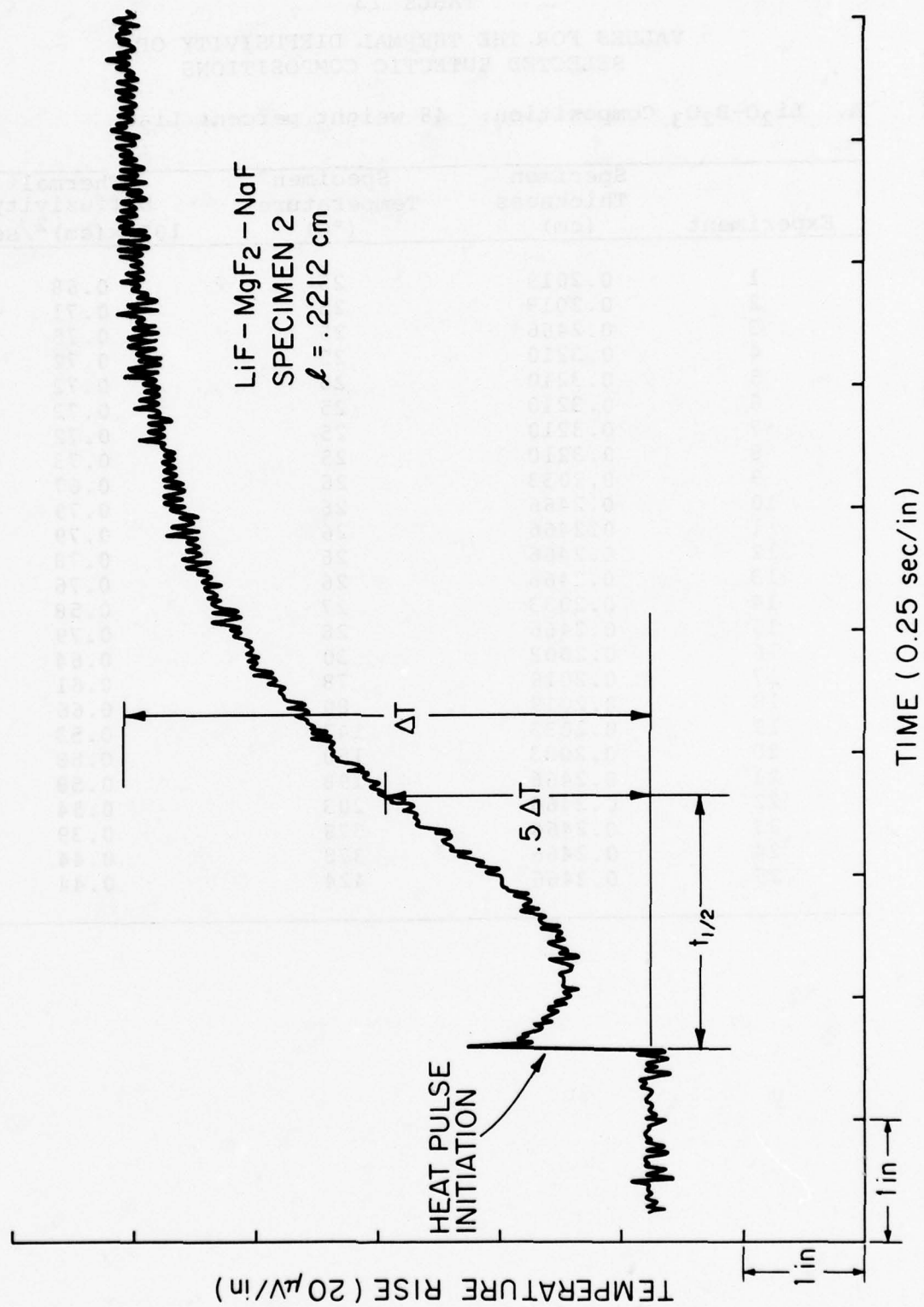
Figure 9.   Typical Plot of the Back Surface Temperature Rise as a Function of Time.

43

TABLE 13

VALUES FOR THE THERMAL DIFFUSIVITY OF
SELECTED EUTECTIC COMPOSITIONS

A. Li_2O-B_2O_3 Composition: 48 weight percent Li_2O

Experiment	Specimen Thickness (cm)	Specimen Temperature (°C)	Thermal Diffusivity $10^{-1} x (cm)^2$/sec
1	0.2019	25	0.68
2	0.2019	25	0.71
3	0.2466	25	0.75
4	0.3210	25	0.72
5	0.3210	25	0.72
6	0.3210	25	0.72
7	0.3210	25	0.72
8	0.3210	25	0.73
9	0.2033	26	0.67
10	0.2466	26	0.79
11	0.2466	26	0.79
12	0.2466	26	0.78
13	0.2466	26	0.76
14	0.2033	27	0.58
15	0.2466	28	0.79
16	0.2002	30	0.64
17	0.2019	78	0.61
18	0.2019	80	0.66
19	0.2033	147	0.53
20	0.2033	150	0.58
21	0.2466	198	0.58
22	0.2466	203	0.54
23	0.2466	378	0.39
24	0.2466	378	0.44
25	0.2466	424	0.44

TABLE 13 (continued)

VALUES FOR THE THERMAL DIFFUSIVITY OF
SELECTED EUTECTIC COMPOSITIONS

B. LiF-MgF$_2$-KF Composition: LiF - 63.5 mole percent

MgF$_2$ - 30.5 mole percent

Experiment	Specimen Thickness (cm)	Specimen Temperature (°C)	Thermal Diffusivity 10^{-1}x(cm)^2/sec
1	0.2531	25	0.17
2	0.2531	25	0.18
3	0.2531	25	0.17
4	0.2531	25	0.17
5	0.2032	25	0.16
6	0.2032	25	0.16
7	0.2032	25	0.16
8	0.2032	25	0.16
9	0.2363	25	0.14
10	0.2363	25	0.14
11	0.2363	25	0.13
12	0.2363	25	0.13
13	0.2060	25	0.16
14	0.2060	25	0.16
15	0.2060	25	0.16
16	0.2060	25	0.16
17	0.2032	39	0.17
18	0.2032	39	0.16
19	0.2060	55	0.12
20	0.2032	57	0.16
21	0.2032	85	0.15
22	0.2060	90	0.13
23	0.2032	127	0.13
24	0.2060	133	0.10
25	0.2060	144	0.12
26	0.2060	171	0.11
27	0.2032	175	0.13
28	0.2060	183	0.11
29	0.2032	207	0.12
30	0.2060	224	0.12
31	0.2032	237	0.12
32	0.2032	271	0.11
33	0.2060	289	0.11
34	0.2060	296	0.10

TABLE 13 (continued)

VALUES FOR THE THERMAL DIFFUSIVITY OF
SELECTED EUTECTIC COMPOSITIONS

B. LiF-MgF$_2$-KF (concluded)

Experiment	Specimen Thickness (cm)	Specimen Temperature (°C)	Thermal Diffusivity 10^{-1}x(cm)^2/sec
35	0.2032	319	0.10
36	0.2060	331	0.12
37	0.2060	346	0.10
38	0.2032	352	0.10
39	0.2060	382	0.10
40	0.2060	391	0.11
41	0.2060	395	0.11
42	0.2032	399	0.09
43	0.2032	400	0.11
44	0.2060	411	0.09
45	0.2060	424	0.12
46	0.2060	451	0.09
47	0.2060	455	0.09

TABLE 13 (continued)

VALUES FOR THE THERMAL DIFFUSIVITY OF SELECTED EUTECTIC COMPOSITIONS

C. LiF-MgF$_2$-NaF Composition: LiF - 59 mole percent

MgF$_2$ - 29 mole percent

Experiment	Specimen Thickness (cm)	Specimen Temperature (°C)	Thermal Diffusivity 10^{-1}x(cm)^2/sec
1	0.2484	25	0.12
2	0.2484	25	0.12
3	0.2484	25	0.14
4	0.2484	25	0.14
5	0.2484	25	0.14
6	0.2484	25	0.13
7	0.2212	25	0.12
8	0.2212	25	0.12
9	0.2212	25	0.12
10	0.2212	25	0.12
11	0.2408	25	0.13
12	0.2408	25	0.13
13	0.2408	25	0.13
14	0.2408	25	0.13
15	0.2431	25	0.14
16	0.2431	25	0.13
17	0.2431	25	0.13
18	0.2431	25	0.14
19	0.2255	25	0.13
20	0.2255	25	0.13
21	0.2255	25	0.13
22	0.2255	25	0.14
23	0.2614	25	0.15
24	0.2614	25	0.16
25	0.2614	25	0.15
26	0.2614	25	0.16
27	0.2212	39	0.17

TABLE 13 (continued)

VALUES FOR THE THERMAL DIFFUSIVITY OF
SELECTED EUTECTIC COMPOSITIONS

C. LiF-MgF$_2$-NaF (concluded)

Experiment	Specimen Thickness (cm)	Specimen Temperature (°C)	Thermal Diffusivity 10^{-1} x (cm)^2/sec
28	0.2484	43	0.18
29	0.2212	60	0.16
30	0.2484	75	0.16
31	0.2212	85	0.15
32	0.2484	103	0.15
33	0.2212	119	0.16
34	0.2212	155	0.15
35	0.2484	155	0.13
36	0.2484	196	0.15
37	0.2484	201	0.12
38	0.2212	210	0.14
39	0.2484	240	0.13
40	0.2212	255	0.13
41	0.2484	275	0.13
42	0.2212	298	0.12
43	0.2484	317	0.11
44	0.2484	328	0.11
45	0.2484	347	0.11
46	0.2212	352	0.11
47	0.2484	391	0.11
48	0.2484	393	0.11
49	0.2212	399	0.11
50	0.2212	445	0.10
51	0.2484	452	0.10
52	0.2212	472	0.09
53	0.2212	479	0.09
54	0.2484	491	0.09

TABLE 13 (continued)

VALUES FOR THE THERMAL DIFFUSIVITY OF
SELECTED EUTECTIC COMPOSITIONS

D. LiF-MgF$_2$ Composition: LiF - 68 weight percent

Experiment	Specimen Temperature (°C)	Thermal Diffusivity 10^{-1}x(cm)^2/sec
A. Specimen Number 1, Thickness= 0.1561 cm		
1	22	0.13
2	24	0.13
3	24	0.14
4	25	0.13
5	25	0.13
6	50	0.12
7	50	0.12
8	78	0.11
9	78	0.11
10	97	0.11
11	97	0.10
12	127	0.10
13	127	0.10
14	149	0.09
15	148	0.09
16	173	0.09
17	173	0.09
18	197	0.08
19	197	0.08
20	230	0.08
21	228	0.08
22	251	0.08
23	252	0.08
24	281	0.08
25	280	0.08
26	298	0.08
27	301	0.08
28	322	0.08
29	323	0.08
30	349	0.08

49

TABLE 13 (concluded)

VALUES FOR THE THERMAL DIFFUSIVITY OF
SELECTED EUTECTIC COMPOSITIONS

D. LiF-MgF$_2$ (concluded)

Experiment	Specimen Temperature (°C)	Thermal Diffusivity 10^{-1}x(cm)^2/sec
A. Specimen Number 1 (concluded)		
31	349	0.08
32	375	0.08
33	380	0.08
34	407	0.08
35	408	0.08
36	431	0.08
37	431	0.08
38	491	0.08
39	490	0.08
40	572	0.07
41	576	0.07
42	625	0.05
43	638	0.05
B. Specimen Number 2, Thickness= 0.2716 cm		
44	26	0.17
45	26	0.16
46	104	0.13
47	106	0.13
48	200	0.11
49	203	0.11
50	309	0.10
51	314	0.09
C. Specimen Number 3, Thickness= 0.2584 cm		
52	32	0.15
53	33	0.15
54	36	0.15

phases, ρ_e and ρ_g. The analytical relation among these parameters is,

$$P = \frac{2\delta}{r} + h \ (\rho_e - \rho_g).$$ (12)

at a fixed immersion depth, h, the pressure is an inverse function of the radius of curvature of the bubble. The maximum pressure is related to the minimum radius of curvature of the bubble which is fixed by the geometry of the tube. The experimental procedure for determining the density consisted of measuring the maximum pressure of the inert gas during the formation and release of the bubble from the end of the capillary tube at a fixed immersion depth. The capillary tube is repositioned at a different depth and the value of the maximum bubble pressure again measured. This experimental data, the maximum bubble pressure versus the immersion depth, are fitted by the method of least squares to a linear equation. The slope of the fitted equation is the value for the difference between the densities of the liquid and inert gas. In all of the experiments either argon or nitrogen was used as the inert gas. Since the value of the density of the liquid is more than 1000 times that of the gas, the value of the slope of the fitted curve was taken as the density of the liquid.

3.4.1 Apparatus and Calibration Tests

The main features of the apparatus which was used for the measurement of the liquid density are illustrated in Figure 10. The capillary tube was mounted on a carriage whose vertical position was controlled by the threaded rod. The D.C. electric motor was energized to turn the threaded rod which changed the vertical position of the capillary tube. The vertical position of the carriage was measured by the potentiometer. The potentiometer was fixed onto the base of the apparatus and the rotor of the potentiometer was connected by a flexible wire to the capillary carriage. The specimen holder was fixed into position within the furnace cavity. The guides insured that the capillary tube and the specimen holder were aligned. The

51
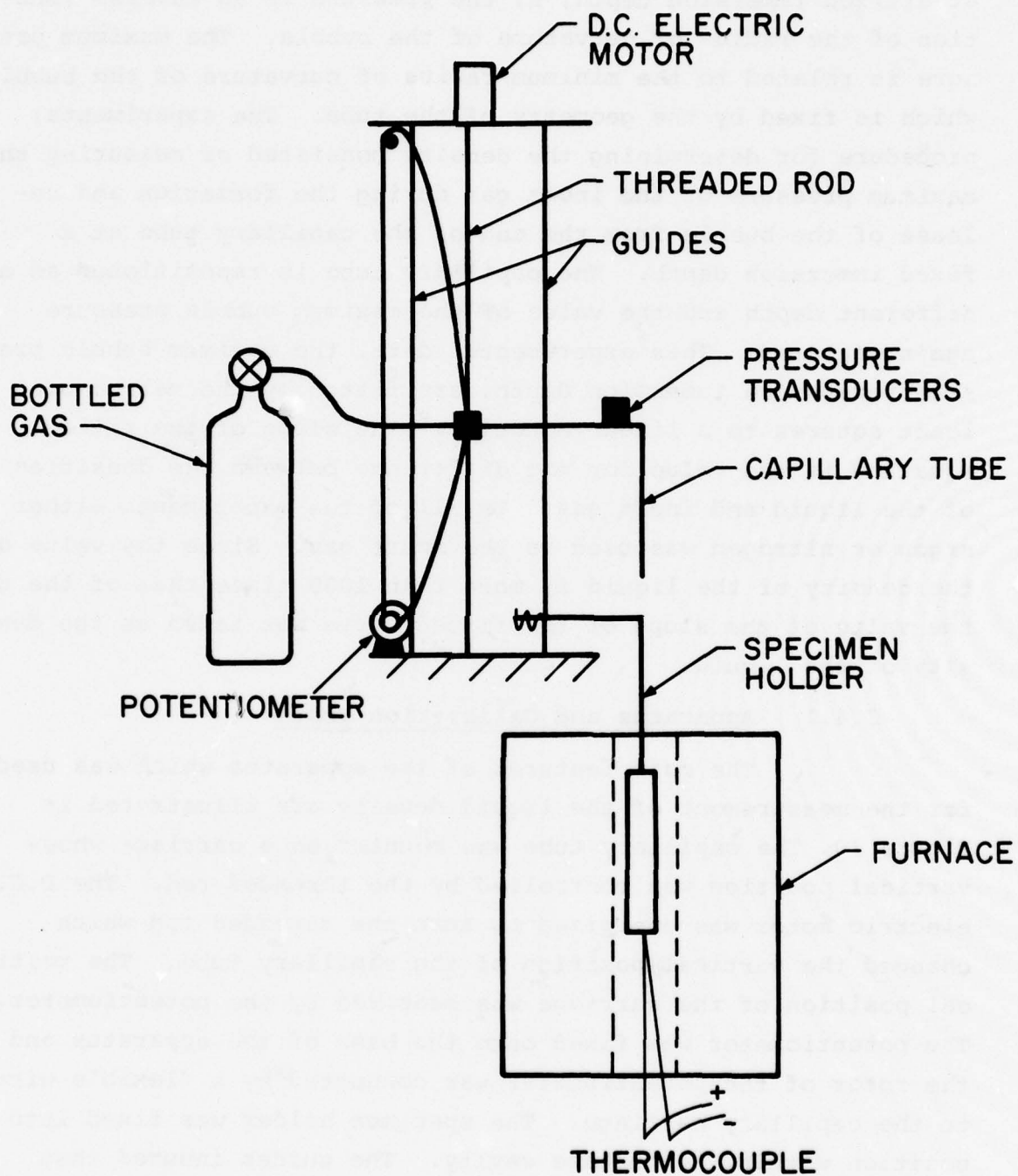
Figure 10. Maximum Bubble Pressure Apparatus for Measurement
of Liquid Densities at Elevated Temperatures.

52

temperature of the specimen was sensed by a chromel-alumel thermocouple which was placed in contact with the specimen holder. The inert gas was either nitrogen or argon. The pressure of the gas and the flow rate were sensed by pressure transducers located in the gas line.

The entire apparatus was calibrated by utilizing distilled water. A distilled water sample was inserted into the specimen holder and the capillary tube was immersed into the water. The pressure of the gas was measured during the bubbling process for two different flow rates. The accepted value for the density of water[*] and the data for the maximum pressure versus the immersion depth were combined with the first derivative of the equation 12 in the form,

$$ K = \frac{1}{\rho_{H_2O}} \frac{\partial P_{max}}{\partial h} \tag{13} $$

to determine the apparatus constant, K. The immersion depth was sensed by a Spectral potentiometer, model number SC-1, whose output was displayed on a Fluke voltmeter, model number 8300A. The pressure and flow rate of the gas were detected by Weston pressure transducers model number 731. The output of these pressure transducers was displayed on a Honeywell X-Y recorder, model number 560. The temperature of the samples was sensed by chromel-alumel thermocouples whose output was displayed on an Omega digital thermometer, model number 2809. The data collected for five different capillaries are presented in Table 14.

The densities of toluene and of methylene chloride were measured at room temperature to provide a check on the accuracy of the experimental procedure. Specimens of reagent grade stock of each of these chemicals were selected and the maximum gas pressure during the bubbling process was measured

---

[*]Handbook of Chemistry and Physics, The Chemical Rubber Company, Cleveland, Ohio, 1968.

TABLE 14

DETERMINATION OF THE APPARATUS CONSTANT, K, FOR THE
LIQUID DENSITY MEASUREMENTS

Probe	Gas	Temperature (°C)	Cycle	$K \left(\dfrac{\text{milliliters}}{\text{grams}} \Big/ \dfrac{\text{millivolts}}{\text{volts}}\right)$
1	nitrogen	24	1	-1.235
			2	-1.251
			3	-1.237
			4	<u>-1.240</u>
				$K_{ave}=$ -1.241
1	argon	20	1	-1.235
			2	-1.238
			3	<u>-1.234</u>
				$K_{ave}=$ -1.236
2	argon	25	1	-1.255
			2	-1.250
			3	<u>-1.247</u>
				$K_{ave}=$ -1.251
3	argon	25	1	-1.249
			2	-1.259
			3	<u>-1.256</u>
				$K_{ave}=$ -1.255
4	argon	24.5	1	-1.245
			2	-1.247
			3	-1.241
			4	<u>-1.243</u>
				$K_{ave}=$ -1.244
5	argon	25	1	-1.246
			2	-1.241
			3	-1.246
			4	<u>-1.239</u>
				$K_{ave}=$ -1.243

54

as a function of immersion depth of the capillary tube. The
density was calculated from the relation,

$$\rho = \frac{1}{K} \frac{\partial P_{max}}{\partial h} \tag{14}$$

where the constant, K, was determined from the calibration
experiments with water. These data are presented in Table 15.
The value of the density of toluene which we measured, 0.8628
grams per milliliter, compares to a value of 0.866 grams per
milliliter which is listed by the Merck Index. The value of the
density for methylene chloride which we measured, 1.311 grams
per milliliter, compares to a value of 1.318 grams per milliliter
as tabulated in the Merck Index. Thus, the accuracy of our
experimental technique in determining the density of a liquid
is greater than 99 percent.

3.4.2   High Temperature Liquid Density Measurements

Measurements were conducted at temperature above
the respective eutectic temperatures for eutectic liquid compo-
sitions in the $Li_2O-B_2O_3$, the $LiF-MgF_2$, the $LiF-MgF_2-KF$, and the
$LiF-MgF_2-NaF$ systems. The results of these measurements are pre-
sented in Table 16. The specimens were contained in an Inconel
617 alloy during the high temperature measurements. The tem-
perature of the furnace was detected with a chromel-alumel
thermocouple whose output was displayed on an Omega Digital
Thermometer, model number 2809. When the specimens were re-
moved from the furnace they were observed to have decreased in
volume during solidification.

3.4.3   Solid Phase Density Data

The values for the densities of the solid phases,
LiF, MgF_2, $NaF \cdot MgF_2$, and $KF \cdot MgF_2$, were determined from X-ray
diffraction studies of the respective unit cells. The value
for the density was calculated by dividing the mass of the unit
cell by the volume of the unit cell. The mass of the unit cell
was obtained by multiplying the molecular weight of the compound

55

TABLE 15

DENSITY MEASUREMENTS FOR TOLUENE AND
METHYLENE CHLORIDE

A. Toluene

Probe Number 1, Nitrogen, Temp.=24°C

Cycle	Density (g/ml)
1	0.8635
2	0.8572
3	0.8678
ave.=	0.8628

B. Methylene Chloride

Probe Number 1, Nitrogen, Temp.=24°C

Cycle	Density (g/ml)
1	1.306
2	1.318
3	1.309
ave.=	1.311

TABLE 16

THE LIQUID DENSITIES OF SELECTED
EUTECTIC COMPOSITIONS

A. $Li_2O-B_2O_3$ eutectic composition – 52 weight percent B_2O_3

Probe Number 3, Argon, Temp.: 710-720°C

Cycle	Density (grams/cc)
1	2.190
2	2.168
3	1.980
4	1.981
5	2.073
6	2.076
7	1.862
8	1.786
9	1.844
10	1.822
11	1.951
12	1.918
13	1.914
14	1.913
15	2.117
16	1.982
Ave.=	1.973 $\pm$ 0.120

TABLE 16   (continued)
THE LIQUID DENSITIES OF SELECTED
EUTECTIC COMPOSITIONS

B. LiF-MgF$_2$-KF eutectic composition (mole fraction):

   LiF-0.635; MgF$_2$-0.305; KF-0.06
   Argon, Temp.: 750°C

Cycle	Probe	Density (grams/cc)
1	3	2.176
2	3	2.180
3	3	2.157
4	3	2.182
5	4	2.167
6	4	2.165
7	4	2.197
8	4	2.201
9	4	2.192
10	4	2.222
11	4	2.197
12	4	2.222
13	4	2.201
14	4	2.162
15	4	2.159
16	4	2.162
17	4	2.158
18	4	2.168
	Ave.=	2.182 ± 0.022

TABLE 16 (continued)

THE LIQUID DENSITIES OF SELECTED
EUTECTIC COMPOSITIONS

C.   LiF-MgF$_2$-NaF Composition (mole fraction):

LiF-0.59; MgF$_2$-0.29; NaF-0.12
Probe Number 3, Argon, Temp.: 760°C

Cycle	Density (grams/cc)
1	2.170
2	2.151
3	2.224
4	2.205
5	2.042
6	2.055
7	2.203
8	2.245
9	2.256
10	2.214
11	2.274
12	2.253
13	2.272
14	2.244
15	2.230
16	2.231
17	2.275
18	2.282
19	2.232
20	2.249
Ave.=	2.215 $\pm$ 0.066

TABLE 16 (concluded)

THE LIQUID DENSITIES OF SELECTED EUTECTIC COMPOSITIONS

D. LiF-MgF$_2$ Composition (weight fraction):

LiF-0.4694; MgF$_2$-0.5306
Probe Number 5, Argon, Temp.: 762°C

Cycle	Density (grams/cc)
1	2.223
2	2.206
3	2.217
4	2.222
5	2.228
Ave.=	2.219

as expressed in grams with the number of formula units per unit cell. The volume of the unit cell was obtained from the measurements of the lattice parameters and the values for the interaxial angles.* The densities of the eutectic mixtures were determined from the values for the densities and compositions of the eutectic constituents. These data for the solid densities at 25°C are presented in Table 17.

---

*Cullity, B.D., Elements of X-ray Diffraction, Addison-Wesley Publishing Company, Inc., Reading, Mass., 1956.

TABLE 17

THE DENSITIES OF SELECTED SOLIDS AT 25°C

A. Pure Compounds*

Component	Crystal System	Unit Cell Parameters x10^{-8}cm	Z formulas per unit cell	Molecular Weight g/mole	Density g/cc
LiF	cubic	a=4.0270	4	25.94	2.638
MgF$_2$	tetragonal	a=4.623 c=3.052	2	62.31	3.172
KF	cubic	a=5.347	4	58.10	2.524
NaF	cubic	a=4.64	4	41.99	2.792
KMgF$_3$	cubic	a=3.9889	1	58.10	3.150
NaMgF$_3$	orthorhombic	a=5.363 b=7.676 c=5.503	4	104.30	3.058
Li$_2$O	cubic	a=4.6114	4	29.88	2.024
B$_2$O$_3$	cubic	a=10.055	16	69.62	1.819
Li$_3$BO$_3$	monoclinic	a=8.337 b=9.179 c=3.260 β=101.60°	4	79.63	2.164
Li$_6$B$_4$O$_9$	monoclinic	a=9.179 b=23.41 c=3.326 β=92.68°	4	28.88	2.129

B. Eutectic Compositions**

System A B C	Composition (weight fraction) A	B	C	Density g/cc
LiF-MgF$_2$-KF	0.4227	0.4878	0.0895	2.918
LiF-MgF$_2$-NaF	0.3983	0.4705	0.1312	2.970
LiF-MgF$_2$	0.4694	0.5306	---	2.897
Li$_2$O-B$_2$O$_3$	0.48	0.52	---	2.147

*Berry, Powder Diffraction File, Joint Committee on Powder Diffraction Standards, 1845 Walnut Street, Philadephia, PA, 1967.

**Evaluation of Eutectic Fluoride Thermal Energy Storage Unit Compatibility, AFAPL-TR-75-92, Part 1.

62

SECTION IV
CONCLUSIONS AND RECOMMENDATIONS

As a result of the review of the thermophysical properties
of the inorganic oxides a total of nine pure inorganic oxides
were identified which have a value for the heat of fusion greater
than 100 watt-hours per pound. However, all of these nine oxides
melt at temperatures greater than 1570°C (see Table 1). The
binary systems of these nine oxides were reviewed to identify
binary compositions which have a liquid-solid transformation
in the temperature interval of 538°C to 760°C. A total of seven
binary systems were identified which contain liquid-solid trans-
formations in the desired temperature interval. An estimated
value for the heat of transformation was performed on all of
these systems. The $Li_2-B_2O_3$ eutectic composition at 48 weight
percent Li_2O was identified to have the highest value (see Table
4). The heat of the transformation of this composition was
measured and the value was significantly lower than the estimated
value. The estimated value was 1.102 K joules per gram. The
measured value was 0.414 K joules per gram. A value for the
heat of transformation of the $LiF-MgF_2-KF$ was measured and
found to be 0.7536 K joules per gram. Thus, the eutectic
fluoride composition was assessed to have a higher potential
than the eutectic oxide composition for application as a heat
energy storage material in the specified temperature interval.
The measured values for the thermal diffusivity of the eutectic
fluoride compositions are higher than the eutectic oxide compo-
sitions for all temperatures up to the transformation temperature
(see Table 13). Measurements of the liquid density were con-
ducted and the oxide composition is less than that of the fluoride
compositions (see Table 15).

The comparison of the heat of transformation for the Li_2O-
B_2O_3 eutectic composition shows that the measured value is only
37.5 percent of the value which was estimated based on the
properties of the pure components.

63

Based on the measured values for the heat of transformation, the eutectic fluoride compositions are recommended for applications in the specified temperature range over the eutectic oxide compositions. However, a study of the compositions of inorganic fluoride-inorganic oxides should be conducted to determine if there are compositions in these reciprocal systems which have values for their heat of transformation which will make them suitable for thermal energy storage applications.

5.1 REVIEW OF LIQUID-SOLID TRANSFORMATIONS OF 53 BINARY INORGANIC OXIDE SYSTEMS

The liquid-solid transformations which are presented in the phase diagrams* of 53 binary inorganic oxide systems are described in the following paragraphs.

$ThO_2-B_2O_3$

This binary system is characterized by two eutectic reactions, the formation of a single intermediate compound, and a syntectic reaction. The syntectic reaction in this system involves the decomposition of the intermediate compound into two immiscible liquids. Specimens which were quenched from the immiscible liquid region were observed to consist of the glassy phase of boron oxide, and the crystalline phases of thoria, and the intermediate compound. There is no evidence of a terminal solid solubility region in either end member. The eutectic transformation which occurs at a temperature of slightly less than 1483°C and at a composition of 80 mole percent thoria represents a substantial decrease in the liquid-solid transformation temperature of thoria (the melting point of pure thoria is reported to be 2952°C). The immiscible liquid phase region of this system is an indication that the heat of mixing is large and positive. The large value of the heat of fusion of thoria, the high concentration of thoria in the high temperature eutectic, the large decrease in the liquid-solid transformation temperature of thoria due to the addition of the boron oxide, and the probable large positive value which can be expected for the heat of mixing recommend this system for a detailed investigation of the effect of ternary additives on the liquid-solid transformation.

---

*Levin, Robbins, and McMurdie, Phase Diagrams for Ceramists, The American Ceramic Society, Columbus, Ohio, 1964. (See also the 1969 and the 1975 Supplements to the basic publication.)

ThO$_2$-BeO

An eutectic reaction has been reported in this system at a temperature of 2375°C and a composition of 87 mole percent thoria. Although the eutectic temperature of this binary system is beyond the temperature range of immediate interest, the large values of the heat of fusion of the two components and the existence of the eutectic transformation recommend this system for further study of the effect of ternary additives on the liquid-solid transformation.

ThO$_2$-SiO$_2$

This system is characterized by the formation of a single intermediate compound which undergoes a peritectic transformation at a temperature of 1975°C, and a monotectic transformation at a temperature of 2000°C.

ThO$_2$-TiO$_2$

The liquidus curve of this system exhibits a minimum at 55 weight percent thoria and at a temperature of 1640°C.

ThO$_2$-UO$_2$

The phase diagram indicates that the two constituents are mutually soluble at all concentrations in both the liquid phase and in the solid phase. The liquidus boundary decreases monotonically from the melting point of thoria to that of uranium dioxide.

ThO$_2$-Y$_2$O$_3$

No liquid-solid transformations have been reported on investigations which have been conducted up to 2200°C.

ThO$_2$-ZrO$_2$

The phase diagram predicts a high temperature solid solubility phase with a liquid-solid transformation at a temperature greater than 2700°C for all binary compositions.

66

BeO-Al$_2$O$_3$

Three compounds are reported in this system, two of which melt congruently at temperatures of 1870°C and 1910°C, the third compound undergoes a peritectic transformation at a temperature of 1980°C. Three eutectic transformations have been reported. The lowest value for the temperature of these eutectics occurs at 1835°C at a composition of ∿75 weight percent alumina.

BeO-BaO

Three compounds are reported in this system, all of which undergo peritectic transformations. The lowest value for the peritectic transformation temperature of these three compounds occurs at 1284°C. An eutectic transformation is reported at 1141°C and ∿10 weight percent beryllia.

BeO-CaO

A peritectic compound has been reported in this system with a transformation temperature of 1384°C. An eutectic transformation occurs at a temperature of slightly less than 1384°C and a composition of 38 weight percent BeO.

BeO-La$_2$O$_3$

Two compounds, both of which undergo peritectic transformation, have been identified. The peritectic transformation temperatures occur at 1371°C and 1514°C. An eutectic composition has been reported at 1371°C and 12.5 weight percent beryllia.

BeO-MgO

This system is a simple binary eutectic system with an eutectic transformation temperature of 1855°C at a composition of 57 mole percent beryllia.

BeO-SiO$_2$

An eutectic transformation has been estimated to occur at 1670°C and 92 weight percent silica.

67

BeO-SrO

Four compounds are depicted in the phase diagram. All of these compounds undergo peritectic transformations. The lowest temperature of these peritectic transformations occurs at 1306°C. An eutectic transformation occurs at 1302°C at 23 weight percent beryllia.

BeO-ThO$_2$

(See ThO$_2$-BeO).

BeO-TiO$_2$

This system is represented by a simple binary eutectic phase diagram with an eutectic temperature of 1670°C at a composition of 17.5 weight percent beryllia.

BeO-UO$_2$

This system is represented by a simple binary eutectic phase diagram with the eutectic temperature of 2175°C at 30 mole percent uranium dioxide. Another investigator places the eutectic point at 2060°C and 35 mole percent uranium dioxide.

BeO-WO$_3$

This system is depicted as a simple eutectic phase diagram with an eutectic temperature of 1185°C at a composition of 60 mole percent tungsten trioxide.

BeO-Y$_2$O$_3$

The limit of the solid solubility of beryllia in yttria is ~41 mole percent at the eutectic temperature. The eutectic point occurs at 1580°C and 65 mole percent beryllia.

BeO-Yb$_2$O$_3$

This system is represented by a simple eutectic phase diagram with an eutectic temperature of 1720°C at a composition of ~65 mole percent beryllia.

68

BeO-ZrO$_2$

This system is represented by a simple eutectic
phase diagram with an eutectic temperature of 2145°C at a compo-
sition of 68 mole percent beryllia.

Li$_2$O-Al$_2$O$_3$

Compositions in the range of 50 to 84 mole percent
alumina have been investigated. Two compounds are reported which
melt congruently at temperatures of 1700°C and 1950°C. An eutec-
tic transformation is reported at 1670°C and 56 mole percent
alumina.

Li$_2$O-B$_2$O$_3$ (See Section 2.1.3)

Li$_2$O-Bi$_2$O$_3$ (See Section 2.1.3)

Li$_2$O-Fe$_2$O$_3$

The binary phase diagram of these two compounds
is a pseudobinary representation. The liquid phases throughout
the diagram and the solid phases in the Fe$_2$O$_3$-rich region are
only approximately represented. Only the region between 0 to 50
mole percent dilithium oxide is presented, and in this region
an eutectic transformation at 1510°C and 40 mole percent dilithium
oxide is depicted.

Li$_2$O-GeO$_2$

Five compounds have been characterized in this
system. The temperature of the lowest melting point among
these five compounds is 955°C for the compound whose composition
is 3 Li$_2$O · 8 GeO$_2$. Five eutectic compositions have been de-
picted in the phase diagram with the lowest melting eutectic
occurring at 930°C at a composition of 90 weight percent germanium
dioxide. The dilithium oxide-rich portion of this diagram has
not been reported.

69

<u>Li$_2$O-MnO</u>

Two compounds have been reported, but no liquid-solid transformations have been observed at a temperature less than 900°C.

<u>Li$_2$O-MoO$_3$</u> (See Section 2.1.3)

<u>Li$_2$O-SiO$_2$</u>

The phase diagram depicts three compounds and two eutectics. The lowest eutectic transformation occurs at 1024°C and 45 weight percent dilithium oxide, the other eutectic occurs at 1028°C and 18 weight percent dilithium oxide. The intermediate compound, Li$_2$O · SiO$_2$, melts congruently at 1201°C. The compound, Li$_2$O · 2 SiO$_2$, melts at 1033°C. The third compound, 2 Li$_2$O · SiO$_2$, has a peritectic transformation at 1255°C.

<u>Li$_2$O-TiO$_2$</u>

The composition range which has been reported is between 0 and 12 weight percent dilithium oxide. An eutectic transformation is indicated at a temperature of 1220°C and a composition of 5 weight percent dilithium oxide. The liquidus indicates a local maximum of 1350°C at a composition of 12 weight percent dilithium oxide.

<u>Li$_2$O-V$_2$O$_5$</u> (See Section 2.1.3)

<u>Li$_2$O-WO$_3$</u> (See Section 2.1.3)

<u>MgO-Al$_2$O$_3$</u>

This system contains one compound, MgO · Al$_2$O$_3$, which melts congruently at 2105°C. The phase diagram shows that this intermediate phase can dissolve a substantial amount of Al$_2$O$_3$ and MgO at high temperatures. Two eutectics are reported, one occurring at 1920°C and 5 mole percent magnesia, the other at 1995°C and 46 weight percent magnesia.

70

MgO-B$_2$O$_3$

The phase diagram depicts a monotectic transformation, a peritectic transformation, two intermediate congruently melting compounds, and two eutectic transformations. The monotectic transformation occurs at 1142°C and the monotectic point is located at 37 weight percent magnesia. The eutectic transformations occur at 1313°C and 56 weight percent magnesia and at 1358°C and 70 weight percent magnesia. The intermediate compounds, 2 MgO · B$_2$O$_3$ and 3 MgO · B$_2$O$_3$, melt congruently at temperatures at 1340°C and 1356°C, respectively. The peritectic transformation occurs at 988°C.

MgO-BaO

The shape of the liquidus indicates a possible eutectic transformation at 1500°C and ∿41 mole percent magnesia.

MgO-BeO

(See BeO-MgO).

MgO-Bi$_2$O$_3$ (See Section 2.1.3)

MgO-CO$_2$

Only a pressure-temperature diagram is presented.

MgO-CaO

An eutectic transformation is depicted at 2370°C and 35 weight percent magnesia.

MgO-CoO

This system exhibits continuous solubility as a function of composition in both the liquid and solid phases at high temperatures. The liquidus boundary decreases monotonically from that of magnesia to that of cobalt oxide. All liquid-solid transformations occur at temperatures greater than 1800°C.

71

MgO-Cr$_2$O$_3$

The phase diagram which is catalogued between 20
and 100 weight percent magnesia shows one intermediate compound
and one eutectic composition. The compound melt congruently at
2400°C. The eutectic transformation occurs at 2350°C and 37
weight percent magnesia.

MgO-Cu$_2$O

The liquidus boundary reaches a minimum at 1190°C
and ~20 mole percent magnesia.

MgO-FeO

The pseudobinary diagram indicates that all liquid-
solid transformations occur at temperatures greater than 1200°C.

MgO-Fe$_2$O$_3$

The phase diagram indicates that all liquid-solid
transformations occur at temperatures greater than 1500°C.

MgO-GeO$_2$

The phase diagram shows three compounds, three
eutectics, and one monotectic. The temperature of the lowest
liquid-solid transformation occurs at the eutectic transforma-
tion located at 1099°C and 8 mole percent magnesia.

MgO-MnO

The location of the liquidus boundary of this
system has been estimated to be above 1550°C for all compositions.

MgO-NiO

The liquid and solid phases exhibit mutual solubi-
lity for all compositions. The liquidus boundary increases
monotonically from the melting point of N:O (2000°C) to that of
magnesia.

72

MgO-P$_2$O$_5$

Three congruently melting compounds and three
eutectics have been identified. The lowest temperature of the
eutectics is at 1150°C and 24 weight percent magnesia. The
lowest temperature of melting of the three compounds is 1165°C
for the composition MgO · P$_2$O$_5$.

MgO-PuO$_2$

The proposed diagram shows only one eutectic trans-
formation at 2000°C and 42 mole percent magnesia.

MgO-SiO$_2$

The phase diagram depicts two compounds, two
eutectic transformations, and one monotectic transformation.
The eutectic transformation at 1543°C and 31 weight percent
magnesia is the lowest temperature of the liquid-solid trans-
formations.

MgO-SrO

The liquidus curve infers an eutectic transforma-
tion at 1950°C and 45 mole percent magnesia.

MgO-Ta$_2$O$_5$

A preliminary phase diagram depicts three compounds
and two eutectics. The compositions and temperatures of the
transformations are uncertain but have been estimated to occur
above 1500°C.

MgO-TiO$_2$

The proposed diagram contains three compounds.
Studies of this system by different investigators are in con-
flict with the type of liquid-solid transformation of the
magnesia-rich compounds. One investigator depicts two peritectic
transformations and one congruently melting compound, which in
earlier investigation depicts all three compounds as congruently

73

melting phases. This investigation also shows four eutectic transformations, whereas the subsequent investigation shows only two eutectic transformations. In any event, all of the liquid-solid transformations occur at temperatures above 1500°C.

$MgO-UO_2$

The eutectic transformation presented in the phase diagram is estimated to occur at 1750°C and 50 mole percent magnesia. The uranium dioxide phase shows extensive solid solubility for magnesia.

$MgO-V_2O_5$ (See Section 2.1.3)

$MgO-WO_3$

One compound and two eutectics are depicted in the phase diagram. The lowest temperature of the liquid-solid transformation occurs at the eutectic composition of 30 mole percent magnesia and at 1120°C.

$MgO-Y_2O_3$

The phase diagram shows one compound and two eutectics. The lowest liquid-solid transformation occurs for the eutectic composition at 50 mole percent magnesia and 1980°C.

$MgO-ZnO$

The phase diagram shows only an eutectic transformation at 1850°C and 30 weight percent magnesia. The magnesia terminal solid solution shows it to have a high solubility for zinc oxide.
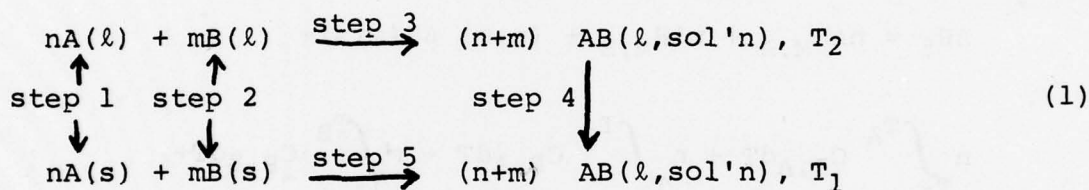
$MgO-ZrO_2$

The eutectic transformation is the only liquid-solid transformation depicted in the phase diagram. The eutectic transformation occurs at 2050°C and 50 mole percent magnesia. Magnesia has a large solubility in the zirconia terminal solid solution.

74

5.2   THE ENTHALPY OF THE LIQUID-SOLID TRANSFORMATION

The amount of heat energy which can be stored or released in the isothermal and reversible transformation between a pure solid and liquid phase at constant pressure is obtained directly from the value for the enthalpy of fusion of the substance. However, when two solid phases of different compositions react to form a single liquid phase, then the value for the enthalpy of mixing must be taken into account to determine the amount of heat energy involved in the liquid-solid transformation.

The effect of the enthalpy of mixing on the energy storage capacity of a liquid-solid transformation can be assessed by consideration of the following thermodynamic cycle. The isothermal and reversible reaction between two solid phases may be considered as the sum of the following processes:

$$
\begin{array}{ccc}
nA(\ell) + mB(\ell) & \xrightarrow{\text{step 3}} & (n+m)\ AB(\ell,\text{sol'n}),\ T_2 \\
\uparrow \qquad \qquad \uparrow & & \Big\downarrow \\
\text{step 1}\quad \text{step 2} & & \text{step 4} \\
\downarrow \qquad \qquad \downarrow & & \\
nA(s) + mB(s) & \xrightarrow{\text{step 5}} & (n+m)\ AB(\ell,\text{sol'n}),\ T_1
\end{array}
\tag{1}
$$

Step 1: Heat "n" moles of component A from temperature T_1 to T_2. The enthalpy change of this step is given by,

$$
\Delta H_1 = n \int_{T_1}^{T_A} C_{P,A} dT + n\Delta H_{M,A} + n \int_{T_A}^{T_2} C_{P,A} dT,
\tag{2}
$$

where T_A represents the melting point of pure A.

Step 2: Heat "m" moles of component B from temperature T_1 to T_2. The enthalpy change for this step is given by,

$$
\Delta H_2 = m \int_{T_1}^{T_B} C_{P,B} dT + m\Delta H_{M,B} + m \int_{T_B}^{T_2} C_{P,B} dT,
\tag{3}
$$

where T_B represents the melting point of pure B.

75

Step 3: React the two separate liquid components to form the AB liquid solution at a temperature of T_2. The enthalpy change for this step is given by,

$$\Delta H_3 = (n+m)\, \Delta H\,(mix). \tag{4}$$

Step 4: Cool the AB liquid solution from temperature T_2 to T_1. The enthalpy change for this step is given by,

$$\Delta H_4 = (n+m) \int_{T_2}^{T_1} C_{P,AB}\,dT. \tag{5}$$

Step 5: The value for the enthalpy of the liquid-solid transformation between the two solid phases, A and B, and the liquid solution, AB, at the temperature, T_1, can be expressed as the sum of the enthalpies of the first four steps, and is as follows,

$$\Delta H_5 = n\Delta H_{M,A} + m\Delta H_{M,B} + (n+m)\, \Delta H(mix) +$$

$$n\int_{T_1}^{T_A} C_{P,A}\,dT + n\int_{T_A}^{T_2} C_{P,A}\,dT + m\int_{T_1}^{T_B} C_{P,B}\,dT +$$

$$m\int_{T_B}^{T_2} C_{P,B}\,dT + (n+m) \int_{T_2}^{T_1} C_{P,AB}\,dT. \tag{6}$$

In the absence of data for the heat capacities of the liquid phase, the Neumann-Kopf Rule states that the heat capacity of a substance may be taken as the sum of the heat capacities of the elemental constituents. The application of this Rule in the present analysis gives a zero value to the sum of heat capacity terms. As a result, the heat energy which can be stored in the isothermal liquid-solid transformation is given by,

$$\Delta H_5 \approx n\Delta H_{M,A} + m\Delta H_{M,B} + (n+m)\, \Delta H(mix). \tag{7}$$

The first two terms on the right-hand side of this expression are properties of the individual components. The last

term on the right is the contribution due to the enthalpy of mixing. The effect of the enthalpy of mixing on the heat of the liquid-solid transformation can be either positive or negative depending on whether the reaction is endothermic or exothermic. If the reaction is endothermic, then the enthalpy of mixing is positive and additional heat energy can be stored in the transformation. If the reaction is exothermic, then the converse is true and less heat energy can be stored in the transformation than would be predicted from the properties of the individual components.